

1 SO₂ photolysis as a source for sulfur mass-independent 2 isotope signatures in stratospheric aerosols

3
4 A. R. Whitehill¹, B. Jiang², H. Guo², and S. Ono¹

5 [1]{Department of Earth, Atmospheric, and Planetary Sciences, Massachusetts Institute of
6 Technology, 77 Massachusetts Ave., Cambridge, MA 02139, USA}

7 [2]{Department of Chemistry and Chemical Biology, University of New Mexico,
8 Albuquerque, NM 87131, USA}

9 Correspondence to: A.R. Whitehill (arwhite@mit.edu)

10

11 Abstract

12 Signatures of sulfur isotope mass-independent fractionation (S-MIF) have been observed in
13 stratospheric sulfate aerosols deposited in polar ice. The S-MIF signatures are thought to be
14 associated with stratospheric photochemistry following stratospheric volcanic eruptions, but
15 the exact mechanism responsible for the production and preservation of these signatures is
16 debated. In order to identify the origin and the mechanism of preservation for these signatures,
17 a series of laboratory photochemical experiments were carried out to investigate the effect of
18 temperature and added O₂ on S-MIF produced by the two absorption band systems of SO₂:—
19 photolysis in the 190 nm to 220 nm region and photoexcitation in the 250 nm to 350 nm
20 region. The SO₂ photolysis (SO₂ + hν → SO + O) experiments showed S-MIF signals with
21 large ³⁴S/³²S fractionation, which increases with decreasing temperature. The overall S-MIF
22 pattern observed for photolysis experiments, including high ³⁴S/³²S fractionations, positive
23 mass-independent anomalies in ³³S, and negative anomalies in ³⁶S, is consistent with a major
24 contribution from optical isotopologue screening effects and measurements—data for
25 stratospheric sulfate aerosols. In contrast, SO₂ photoexcitation produced products with
26 positive MIF anomalies in both ³³S and ³⁶S that is different from stratospheric aerosols. SO₂
27 photolysis in the presence of O₂ produced SO₃ with S-MIF signals, suggesting the transfer of
28 the MIF signals of SO to SO₃ by the SO + O₂ + M → SO₃ + M reaction. This is supported with
29 energy calculations of stationary points on the SO₃ potential energy surfaces, which indicate

1 that this reaction occurs slowly on a single adiabatic surface, but that it can occur more
2 rapidly through intersystem crossing. Based on our experimental results, we estimate a
3 termolecular rate constant on the order of $10^{-37} \text{ cm}^6 \text{ molecule}^{-2} \text{ s}^{-1}$.~~The results from our~~
4 ~~experiments constrain the termolecular reaction rate to between $1.0 \times 10^{-37} \text{ cm}^6 \text{ molecule}^{-2} \text{ s}^{-1}$~~
5 ~~and $1.0 \times 10^{-36} \text{ cm}^6 \text{ molecule}^{-2} \text{ s}^{-1}$.~~ This rate can explain the preservation of mass independent
6 isotope signatures in stratospheric sulfate aerosols and provides a minor, but important,
7 oxidation pathway for stratospheric SO₂ ~~above about 25 km altitude~~. The production and
8 preservation of S-MIF signals in the stratosphere requires a high SO₂ column density to allow
9 for optical isotopologue screening effects to occur and to generate a large enough signature
10 that it can be preserved. In addition, the ~~and an~~ SO₂ plume must reach an altitude of around
11 20 to 25 km, where SO₂ photolysis becomes a dominant process ~~reaching an altitude of 25 km~~
12 and higher. ~~These experiments are the first step towards understanding the origin of the sulfur~~
13 isotope anomalies in stratospheric sulfate aerosols.

Formatted: Subscript

15 1 Introduction

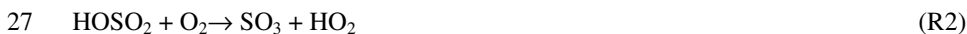
16 Explosive volcanic eruptions that inject sulfur dioxide (SO₂) into the stratosphere can
17 cause perturbations to the stratospheric sulfur cycle for years following eruptions. The
18 increase in stratospheric sulfate aerosols associated with injections of SO₂ result in
19 stratospheric warming and tropospheric cooling, and can also trigger changes in atmospheric
20 circulation and increases in ozone depletion (Robock, 2000). Perturbations to the stratospheric
21 sulfur cycle following large volcanic eruptions are recorded as changes in sulfur isotope
22 ratios, as measured in stratospheric sulfate aerosol samples (Castleman et al., 1974), as well as
23 in ice core records (Savarino et al., 2003; Baroni et al., 2007).

Formatted: Indent: First line: 0.3"

24 The reaction with OH is the dominant oxidation pathway for SO₂ in the stratosphere:



26 This reaction is followed by:



28 In the presence of H₂O, SO₃ readily forms sulfuric acid (H₂SO₄) via:



Formatted: Indent: First line: 0.49"

1 Ab-initio transition state theory calculations of the isotope effect for OH oxidation (R1) predict that $^{34}\text{SO}_2$ is oxidized 0.9% slower than $^{32}\text{SO}_2$ (Tanaka et al., 1994), although
2 calculations with RRKM theory predicts an inverse isotope effect, in which $^{34}\text{SO}_2$ reacts 12%
3 to 15% faster than $^{32}\text{SO}_2$ (Leung et al., 2001). Experimental studies of OH oxidation
4 (R1) showed an inverse isotope effect, but with a smaller magnitude, with $^{34}\text{SO}_2$ reacting
5 about 1% faster than $^{32}\text{SO}_2$ (Harris et al., 2012). ~~Although the~~ experimentally measured
6 isotope effect ~~is in~~ might be sufficient to explain the roughly 2% enrichment in $\text{H}_2^{34}\text{SO}_4$
7 relative to $\text{H}_2^{32}\text{SO}_4$ following the major Mt. Agung (1963) eruption (Castleman et al., 1974),
8 the large observed isotope effect suggests the possibility of an additional oxidation reaction
9 with larger ^{34}S fractionations.

10 ~~_____ An additional oxidation reaction is necessary to explain the sulfur isotope effects in~~
11 ~~stratospheric sulfate aerosols following large volcanic eruptions.~~

13 An additional unexplained observation is the isotope anomalies in $^{33}\text{S}/^{32}\text{S}$ and $^{36}\text{S}/^{32}\text{S}$ ratios
14 relative to $^{34}\text{S}/^{32}\text{S}$ ratios. These signatures of mass-independent fractionation (MIF) have been
15 observed in ice cores associated with large volcanic eruptions (Savarino et al., 2003; Baroni
16 et al., 2007, 2008; Lanciki, 2010; Lanciki et al., 2012). Ice core sulfate peaks are commonly
17 used to reconstruct the impact of past volcanic activity, which is critical to forcing climate
18 models (Robock, 2000). For several years following large injections of SO_2 into the
19 stratosphere, stratosphere-derived sulfate can dominate sulfate deposition in ice cores and,
20 ~~when~~ corrected for background levels, can preserve the sulfur isotopic composition of
21 stratospheric sulfate aerosols. Experimental studies demonstrate that OH oxidation of SO_2
22 (R1) does not produce mass-independent sulfur isotope anomalies (Harris et al., 2012, 2013),
23 so an additional oxidation mechanism is required to produce the mass-independent sulfur
24 isotope signatures. Three reactions have been proposed to explain these isotope anomalies:
25 excited-state photochemistry of SO_2 in the 250 nm to 350 nm absorption region (Savarino et
26 al., 2003; Hattori et al., 2013), SO_2 photolysis in the 190 nm to 220 nm absorption region
27 (Ono et al., 2013), and SO_3 photolysis (Pavlov et al., 2005).

Formatted: Indent: First line: 0.49"

28 We present results of laboratory photochemical experiments that support SO_2
29 photolysis as the main source for the MIF signatures observed in stratospheric sulfate aerosols
30 following some large (stratospheric) volcanic eruptions. In particular, SO_2 photolysis
31 produces large MIF anomalies, as well as large mass-dependent isotope fractionations
32 (Masterson et al., 2011; Whitehill and Ono, 2012; Ono et al., 2013) that are consistent with

1 the isotopic signatures observed in stratospheric sulfate aerosols in ice cores (Ono et al.,
2 2013). ~~Even a minor contribution of SO₂ photolysis to the production of sulfate aerosols can~~
3 ~~have a major influence on the isotope ratios of sulfur.~~

4 Photolysis of SO₂ occurs above around 20 to 25 km in the wavelength region of 190
5 nm to 220 nm, which lies in the spectral window between the Schumann-Runge absorption
6 edge of oxygen (O₂) and the Hartley bands of ozone (O₃). SO₂ photolysis produces sulfur
7 monoxide (SO) and O(³P) via the following reaction:



9 It is generally accepted that this reaction is followed by rapid oxidation of SO to SO₂
10 via (Black et al., 1982; Savarino et al., 2003; Pavlov et al., 2005):



12 Reactions R4 and R5 combine to form a null cycle for sulfur, but catalyze the formation of
13 odd oxygen (Bekki, 1995). If SO is completely oxidized to SO₂, no isotopic signature from
14 SO₂ photolysis can be preserved (Pavlov et al., 2005).

15 We propose an additional channel where SO is oxidized directly to SO₃ via the
16 termolecular reaction:



18 A previous study by Black et al. (1982) showed that the maximum termolecular rate constant
19 for reaction R6 is 10⁻³⁶ cm⁶ molecule⁻² s⁻¹. This rate is considered too slow to play an
20 important role for stratospheric chemistry (Black et al., 1982). However, given the large
21 isotope effects produced during SO₂ photolysis, even a minor contribution from R6 will
22 produce a significant signal on the sulfur isotopic composition of stratospheric sulfate
23 aerosols.

24 We present results from laboratory photochemical experiments that investigate the effect
25 of temperature and molecular oxygen on the isotope effects produced during SO₂ photolysis
26 (190 nm to 220 nm) and SO₂ photoexcitation (250 nm to 350 nm). Using the results of the
27 experiments in the presence of molecular oxygen, we calculate a lower bound estimate on the
28 rate of R6. In addition, our proposal is further supported by ab-initio calculations of
29 stationary points along the potential energy surfaces (PESs) for the SO oxidation reactions
30 (R5 and R6). Finally, we present a simple steady state photochemical model to show that the

Formatted: Indent: First line: 0.49"

Formatted: Indent: First line: 0.49"

Formatted: Indent: First line: 0.3"

1 rate constraints on reaction R6 are sufficient for it to make a significant contribution to the
2 isotopic signature of stratospheric sulfate aerosols during volcanically perturbed periods.

3 **2 Methods**

4 **2.1 Photochemical reaction set-up**

5 Conditions for all photochemical experiments are listed in Table 1. All experiments were
6 performed in a cylindrical glass photochemical reaction cell with a pathlength of 15.3 cm and
7 an inner diameter of 5.2 cm (Ono et al., 2013). Temperature-controlled experiments were
8 performed in a jacketed cell of the same dimensions. The front window of the cell was made
9 of UV-grade SiO₂ (Corning 7980) with greater than 90% transmittance above-at wavelengths
10 longer than 190 nm. The window was sealed to the cell with an o-ring and held in place
11 securely with a plastic clamp. Temperature-controlled experiments also utilized a second pre-
12 cell (5.3 cm pathlength) attached to the front window of the reaction cell and held under
13 vacuum. The purpose of the pre-cell was to thermally insulate the front window and prevent
14 condensation from occurring on the front window during low temperature experiments.

15 A series of mass-flow controllers controlled the flow rate of gases into the cell. Gas entered
16 the cell through an inlet at the rear of the cell (for temperature cell experiments) or the front of
17 the cell (for other experiments) and exited the cell through an outlet at the opposite end of the
18 cell. An 8 cm to 10 cm length of glass tubing packed with glass wool was placed
19 immediately after the cell exit to trap aerosols formed within the cell. Following the aerosol
20 trap, the gas was flowed through a proportionating valve to a vacuum pump. A capacitance
21 manometer placed before the entrance to the cell monitored the pressure within the cell. The
22 proportionating valve was used to control the pressure within the cell to within 30 Pa of a
23 setpoint pressure, which was usually 101.3 kPa.

24 Prior to each temperature-controlled experiment, the reaction cell was flushed with
25 nitrogen(N₂) for several hours and the chiller was allowed to reach its setpoint temperature
26 and equilibrate for at least an hour. The temperature of the reaction cell was calibrated
27 relative to the chiller setpoint temperature on two occasions using a series of K-type
28 thermocouples suspended within the cell. During calibrations, N₂(without SO₂) was flowed
29 through the cell at a rate of 3.33 cm³ s⁻¹ (200 sccm, standard cubic centimeter per minute).
30 Thermocouples placed at the front and rear of the cell gave consistent measurements to within

Formatted: Subscript

1 5 K, with a higher gradient at lower temperatures. No significant differences were observed
2 between the two calibrations. Results for the temperature calibration are shown in Figure 1.

3 **2.2 Temperature effect on SO₂ photolysis (190 nm to 220 nm) and** 4 **photoexcitation (250 nm to 350 nm)**

5 The temperature effect on SO₂ photolysis (190 nm to 220 nm) was ~~measured~~-tested using the
6 temperature-controlled reaction cell described in Section 2.1. Experiments were performed in
7 a nitrogen-flushed glove box to prevent the spectral interference from the Schumann-Runge
8 band of oxygen (O₂). A 200 W deuterium (D₂) arc lamp (D 200 F, HeraeusNoblelight) was
9 used as the light source without optical filters. The output from the lamp was collimated
10 using a fused silica plano-convex lens. 1000 ppm SO₂ (in N₂) was flowed through the cell at
11 a rate of 3.33 cm³ s⁻¹ (200 sccm) for all experiments, and pressure within the cell was held
12 constant at 101.3 kPa, giving an SO₂ partial pressure of 0.10 kPa within the cell.

13 Following photolysis experiments, the cell was removed from the glove box and rinsed well
14 with dichloromethane (~~DCM~~) to dissolve any elemental sulfur that was formed. The glass
15 wool in the aerosol trap was also collected and rinsed with ~~DCM~~dichloromethane. Elemental
16 sulfur was recrystallized from ~~DCM~~dichloromethane and converted to silver sulfide using the
17 reduced chromium chloride method (Whitehill and Ono, 2012; Canfield et al., 1986).
18 Multiple sulfur isotope ratios were measured as described in Section 2.4.

19 Photoexcitation experiments were performed in a room air atmosphere using a 150 W UV-
20 enhanced xenon (Xe) arc lamp (Newport Model 6254) housed in a lamp housing (Newport
21 Model 67005), which focused and collimated the light to a 3.3 cm diameter beam. The light
22 was passed through a liquid filter (Newport Model 51945) filled with deionized (18.2 MΩ)
23 water and a 250 nm longpass filter (Asahi Spectra, ZUL0250).

24 Following Whitehill et al. (2013), acetylene (C₂H₂) was used to trap triplet excited-state SO₂
25 (³SO₂). During experiments, 5% SO₂ (in N₂), pure C₂H₂ (Atomic Absorption Grade), and
26 pure N₂ (Ultra High Purity grade) were flowed through the cell continuously at a rate of 0.67
27 cm³ s⁻¹ (40 sccm), 0.03 cm³ s⁻¹ (2 sccm), and 2.63 cm³ s⁻¹ (158 sccm), respectively. Pressure
28 in the cell was held constant at 101.3 kPa, giving a total flow rate of 3.33 cm³ s⁻¹, an SO₂
29 partial pressure of 1.01 kPa, and a C₂H₂ partial pressure of 1.01 kPa within the cell during the
30 experiments.

1 Following the experiments, the interior walls of the cell and the window were rinsed with
2 ethanol and water to dissolve any organosulfur products formed. The glass wool in the
3 aerosol trap was also collected. The organosulfur aerosol products were converted to silver
4 sulfide using the Raney nickel hydrodesulfurization method of Oduro et al. (2011). Multiple
5 sulfur isotope ratios were measured as described in Section 2.4.

6 **2.3 SO₂ photochemistry in the presence of O₂**

7 The photochemistry of SO₂ + O₂ with ultraviolet radiation was studied using a reaction cell at
8 room temperature. The 150 W Xe arc lamp (described in Section 2.2) was used as the light
9 source without the liquid filter. Several experiments were performed with a 200 ± 35 nm
10 bandpass filter (Model 200-B, Acton Research, Acton, MA), a 250 nm longpass filter (Asahi
11 Spectra, ZUL0250), or a 280 nm (285 nm cut-on) longpass filter (Newport Model FSR-
12 WG280) to isolate particular absorption bands of SO₂, but most experiments were performed
13 with the Xe lamp and no filters (Table 1).

14 Following experiments, the cell was rinsed well first with dichloromethane (~~DCM~~) then with
15 water. Although sulfate was the dominant product, the cell was rinsed well with
16 ~~dichloromethane-DCM~~ first to ensure the removal of elemental sulfur. For two experiments
17 performed with no oxygen, elemental sulfur was recovered. After rinsing the cell with water,
18 5.0 cm³ of a 1.0 mol dm⁻³ solution of barium chloride (BaCl₂) was added to the water used to
19 rinse the cell to precipitate sulfate as barium sulfate. Barium sulfate was rinsed several times
20 with deionized water and dried. The glass wool inside the aerosol trap was combined with the
21 barium sulfate and all sulfate was converted to silver sulfide using the method of Forrest and
22 Newman (1977). Multiple sulfur isotope ratios were measured as described in Section 2.4.

23 **2.4 Isotope analysis of photochemical products**

24 Photochemical products were converted to silver sulfide (Ag₂S). Ag₂S was rinsed well three
25 to four times with deionized water and then dried completely at 353 K. Dried Ag₂S was
26 weighed for total yield and about 8 μmol of Ag₂S was weighed into an aluminum foil capsule
27 for isotope analysis. Capsules were loaded into nickel reaction chambers and reacted under
28 approximately 7.3 kPa of fluorine gas (F₂) for at least 8 hours at 573 K. The resultant SF₆
29 was purified cryogenically and by gas chromatography. Isotope ratios of pure SF₆ were
30 measured as SF₅⁺ ions using a Thermo Scientific MAT 253 Isotope Ratio Mass Spectrometer.

1 For samples where less than 1.6 μmol of Ag_2S was recovered, a microvolume (0.4 cm^3
2 volume) coldfinger was used to concentrate the samples for analysis.

3 Replicate analyses ($N = 28$) of the reference material IAEA-S-1 gave 2σ standard
4 deviations of 0.26 ‰ for $\delta^{34}\text{S}$, 0.014 ‰ for $\Delta^{33}\text{S}$, and 0.19 ‰ for $\Delta^{36}\text{S}$ for standard isotope
5 ratio mass spectrometry analysis. Microvolume analyses for smaller samples gave 2σ
6 standard deviations for replicate analyses of IAEA-S-1 ($N = 14$) of 0.9 ‰ for $\delta^{34}\text{S}$, 0.08 ‰ for
7 $\Delta^{33}\text{S}$, and 0.8 ‰ for $\Delta^{36}\text{S}$. Replicate experiments performed under identical conditions had
8 differences larger than the analytical uncertainty, suggesting experimental variability was the
9 dominant source of uncertainty in our measurements.

10 2.5 Potential energy surfaces of $\text{SO} + \text{O}_2 \rightarrow \text{SO}_3 \rightarrow \text{SO}_2 + \text{O}$ reactions

11 To test the feasibility of reaction R6, ab-initio energy calculations at multiple levels of theory
12 were performed to search important stationary points on the SO_3 potential energy surfaces
13 (PESs). The lowest $\text{SO}({}^3\Sigma^-) + \text{O}_2({}^3\Sigma_g^-)$ asymptote of the SO_3 PESs involves three degenerate
14 states, namely the singlet, triplet, and quintet states. The singlet state corresponds to the
15 ground state of the SO_3 molecule (${}^1\text{A}_1'$), but does not dissociate to the ground state products
16 $\text{SO}_2({}^1\text{A}_1) + \text{O}({}^3\text{P})$ but to $\text{SO}_2({}^1\text{A}_1) + \text{O}({}^1\text{D})$. The triplet surface corresponds to the ground
17 state products but is adiabatically associated with a higher energy excited-state (triplet) SO_3 .
18 The quintet state is much higher in energy than the other two states except at the $\text{SO}({}^3\Sigma^-) +$
19 $\text{O}_2({}^3\Sigma_g^-)$ asymptote and will thus not be considered in this study.

20 The B3LYP density functional (Becke, 1988; Lee et al., 1988) was initially used to optimize
21 each minimum and/or transition state on the singlet and triplet potential energy surfaces PESs.
22 Single point calculations at these stationary points were then carried out using an explicitly
23 correlated version of the unrestricted coupled cluster method with single, double and
24 perturbative triple excitations method (UCCSD(T)-F12a; Knizia et al., 2009).

25 In addition, complete active space self-consistent field (CASSCF) calculations were
26 performed (Knowles and Werner, 1985, 1988). Multi-reference Rayleigh Schrödinger
27 perturbation theory of second order (RSPT2 or CASPT2) calculations (Celani and Werner,
28 2000) were performed based on the CASSCF wavefunctions in order to account for part of
29 the dynamical correlation. Calculations including the full valence orbitals would involve 24
30 electrons in 16 orbitals and were not feasible. Instead, the 2s orbital for O and the 3s orbital
31 for S were closed, resulting in an active space of 16 electrons in 12 orbitals (16e,12o).

1 Dunning's augmented correlation-consistent polarized valence triplet-zeta (aug-cc-pVTZ)
2 basis set was used in all cases (Dunning, 1989). B3LYP calculations were performed with
3 Gaussian09 (Frisch et al., 2009) and the other calculations were performed using
4 MOLPRO(Werner et al., 2012).

5 2.6 Definitions

6 Isotopic results will be presented with conventional δ notation, as relative deviations of
7 isotope ratios with respect to reference sulfur.

$$8 \quad \delta^x S = \frac{{}^x R_{\text{product}}}{{}^x R_{\text{reference}}} - 1 \quad (1)$$

9 where $x = 33, 34,$ or 36 and ${}^x R$ is the ratio of ${}^x S$ to ${}^{32} S$ in the substance. For experimental
10 results all isotope ratios will be normalized to the isotope ratios of the initial SO_2 . For natural
11 samples (i.e. stratospheric sulfate aerosol samples), the reference is Vienna Canyon Diablo
12 Troilite (V-CDT).

13 Mass-independent isotope fractionations in ${}^{33} S/{}^{32} S$ and ${}^{36} S/{}^{32} S$ ratios (relative to ${}^{34} S/{}^{32} S$ ratios)
14 will be presented as $\Delta^{33} S$ and $\Delta^{36} S$ values, respectively. These are defined as:

$$15 \quad \Delta^{33} S = \frac{(\delta^{33} S + 1)}{(\delta^{34} S + 1)^{0.515}} - 1 \quad (2)$$

16 and

$$17 \quad \Delta^{36} S = \frac{(\delta^{36} S + 1)}{(\delta^{34} S + 1)^{1.90}} - 1 \quad (3)$$

18 Almost all physical, chemical, and biological processes fractionate isotopes mass-dependently
19 | (i.e. $\Delta^{33} S$ and $\Delta^{36} S$ are approximately equal to $= 0$ and $\Delta^{36} S = 0$). SO_2 photochemistry, as
20 | well as the photochemistry of other sulfur gases such as CS_2 , are some of the few exceptions
21 | that have been shown to produce mass-independent fractionation. Therefore, non-zero $\Delta^{33} S$
22 | and $\Delta^{36} S$ values can be unique tracers of photochemical processes.

23 3 Results

24 All experiments performed are summarized in Table 1. Results from temperature
25 experiments on SO_2 photolysis and SO_2 photoexcitation are given in Tables 2 and 3, whereas

1 results from SO₂ + O₂ experiments are presented in Tables 4 and 5. Tables 6, 7, and 8 give
2 the results from energy calculations on the [potential energy surfaces \(PESs\)](#) of SO₃.

3 3.1 Temperature experiments

4 Results from the temperature experiments (Section 2.2) are shown in Figure 2. The SO₂
5 photolysis (190 nm to 220 nm) experiments (Table 2) revealed that the magnitude of the
6 isotope effects increase with decreasing temperatures, from 129‰ to 191‰, 5.5‰ to 9.1‰
7 and -24.1‰ to -35.8‰, for δ³⁴S, Δ³³S, and Δ³⁶S, respectively. The relationship between
8 isotopes (i.e. Δ³³S versus δ³⁴S and Δ³⁶S versus Δ³³S) did not change significantly as
9 temperature was decreased (0.04 to 0.05 for Δ³³S/δ³⁴S and -3.9 to -4.6 for Δ³⁶S/Δ³³S).

10 [Variability between duplicate experiments also increased at lower temperatures, highlighting](#)
11 [the difficulty of the low temperature experiments and indicating a strong sensitivity to](#)
12 [experimental conditions.](#)

13 SO₂ photoexcitation (250 nm to 350 nm) show decreasing magnitude Δ³³S and Δ³⁶S values at
14 lower temperatures (22.8‰ to 19.0‰ and 52.5‰ to 46.0‰ for Δ³³S and Δ³⁶S, respectively;
15 Table 3). Even at lower temperatures, the product from SO₂ photoexcitation experiments
16 show positive Δ³³S and Δ³⁶S values, as shown previously in room-temperature experiments
17 (Whitehill and Ono, 2012; Whitehill et al., 2013). [As discussed previously \(Whitehill et al.,](#)
18 [2013\), these signatures do not match predictions from isotopologue-specific absorption cross-](#)
19 [sections \(Danielache et al., 2012\), suggesting an additional isotope effect beyond differences](#)
20 [in the initial excitation for different isotopologues.](#)

21 3.2 Oxygen experiments

22 SO₂ photolysis and photoexcitation in the presence of molecular oxygen (O₂) produced mass-
23 independent sulfur isotope signatures in sulfate products (Tables 4 and 5). Isotope ratios of
24 this product sulfate are shown in Figure 3 and compared with stratospheric sulfate aerosol
25 data from ice cores (Savarino et al., 2003; Baroni et al., 2007, 2008; Lanciki, 2010; Lanciki et
26 al., 2012). Strong agreement between the Xe lamp data, 200 nm bandpass (200 BP) data, and
27 previous SO₂ photolysis data (Ono et al., 2013) suggest an SO₂ photolysis source for the
28 isotope effects during broadband SO₂ irradiation with the Xe lamp light source.

29 Experiments focusing on the photoexcitation band of SO₂ using the 250 nm longpass filter
30 (250 LP) and 280 nm longpass filter (280 LP) display a different isotope signature,

1 characterized by positive $\Delta^{33}\text{S}$ and $\Delta^{36}\text{S}$ values, whereas sulfate from SO_2 photolysis has
2 positive $\Delta^{33}\text{S}$ and negative $\Delta^{36}\text{S}$ values. This is consistent with previous findings (Whitehill
3 and Ono, 2012; Whitehill et al., 2013), and demonstrates the MIF in this band region is not
4 produced by chemistry related to acetylene nor oxygen. However, the magnitude of the sulfur
5 MIF signatures (i.e. $\Delta^{33}\text{S}$ and $\Delta^{36}\text{S}$ values) are considerably smaller than previous experiments
6 using C_2H_2 (Table 3, Whitehill et al., 2013). This suggests that a considerable amount of the
7 sulfate in the system is being produced by a mass-dependent process, such as $\text{SO}_2 + \text{SO}_2 \rightarrow$
8 $\text{SO} + \text{SO}_3$ (Whitehill and Ono, 2012). This would dilute the MIF signature. In addition, there
9 is considerable variability (i.e. a factor of ~ 2) was observed between the two 250 nm longpass
10 filter experiments, despite identical experimental conditions. The cause of this variability is
11 uncertain but could relate to the amount of water vapor within the system.

12 3.3 Potential energy surfaces of SO_3

13 Asymptotic energies of $\text{SO}+\text{O}_2$ on each ~~potential energy surface~~ PES were compared with the
14 energies obtained by separate calculations of each species with a certain spin (Table 6). The
15 CASSCF results correctly produced degenerate energies for the $\text{SO}+\text{O}_2$ asymptote on the
16 singlet and triplet states, which exactly match the sum of the energies of ~~the~~ the $\text{SO}(^3\Sigma^-)$ and
17 $\text{O}_2(^3\Sigma_g^-)$ species calculated separately. The CASPT2 results also showed the correct degenerate
18 behavior but the energies shift slightly from those calculated separately, which presumably
19 arises from the perturbative treatment in CASPT2. On the other hand, the UCCSD(T)-F12a
20 and B3LYP results both attribute $\text{SO}+\text{O}_2$ on the singlet state to $\text{SO}(^1\Delta)+\text{O}_2(^1\Delta_g)$, and B3LYP
21 even gives a qualitatively incorrect energy for $\text{SO}+\text{O}_2$ on the triplet state, while UCCSD(T)-
22 F12a attributes the triplet state ~~this one~~ to $\text{SO}(^1\Delta)+\text{O}_2(^3\Sigma_g^-)$. An important conclusion from
23 these data is that one has to use a multi-reference method if ~~an~~ accurate global adiabatic
24 ~~potential energy surface~~ PES is desired for this system. Otherwise, the asymptotic behavior
25 can be completely wrong. None of the previous studies has noticed this, and as a result a
26 single-reference method was always selected (Jou et al., 1996; Martin, 1999; Goodarzi et al.,
27 2010; Ahmed, 2013). Fortunately, single reference methods can accurately describe the PES
28 away from the $\text{SO}+\text{O}_2$ region; they are capable of describing several SO_3 isomers and the
29 SO_2+O product channel reasonably well.

30 Energies for the stationary points computed using multi-reference approaches are reported
31 relative to that of the $\text{SO}(^3\Sigma^-)+\text{O}_2(^3\Sigma_g^-)$ asymptote. However, the active space used in our
32 CASSCF calculations is not sufficient to provide quantitatively accurate results, but a larger

Formatted: Justified

1 active space is still computationally infeasible. For single-reference calculations, we chose to
2 use the UCCSD(T) energies at optimized B3LYP geometries for the stationary points. To
3 avoid the aforementioned problems in the $\text{SO}({}^3\Sigma^-)+\text{O}_2({}^3\Sigma_g^-)$ asymptote, we have used the
4 UCCSD(T) energy sum of the two reactants with the correct spins calculated separately, which
5 has been shown [above](#) to be accurate. The sum of these two energies thus provides the
6 reference for other stationary points on both singlet and triplet PESs. All energies of
7 stationary points are listed in Tables 7 and 8, and the reaction pathways on both PESs are
8 shown graphically in Figure 4, using the energies of the UCCSD(T)//B3LYP calculations. It is
9 seen from Tables 7 and 8 that the experimental derived energy differences (from Chase, 1986)
10 between reactants and products for the $\text{SO}({}^3\Sigma^-)+\text{O}_2({}^3\Sigma_g^-)\rightarrow\text{SO}_3({}^1A_1')$ reaction (-411.29 kJ
11 mole^{-1}), the $\text{SO}({}^3\Sigma^-)+\text{O}_2({}^3\Sigma_g^-)\rightarrow\text{SO}_2({}^1A_1)+\text{O}({}^3P)$ reaction (-54.56 kJ mole^{-1}) and the $\text{SO}({}^3\Sigma^-)$
12 $+\text{O}_2({}^3\Sigma_g^-)\rightarrow\text{SO}_2({}^1A_1)+\text{O}({}^1D)$ reaction (135.27 kJ mole^{-1}) are reproduced well by the
13 UCCSD(T)-F12a//B3LYP calculations, while the other methods contain significant errors.

14 4 Discussion

15 4.1 Origin of mass-independent fractionation during SO_2 photochemistry

16 ~~Isotopologue-specific absorption cross sections are expected to correctly predict the isotope~~
17 ~~effects from SO_2 -photolysis (in the 190 nm to 220 nm region) but fail to reproduce the isotope~~
18 ~~effects from SO_2 photoexcitation (in the 250 nm to 350 nm region). This is due to the~~
19 differences in the photophysics and photochemistry between the photolysis region (190 nm to
20 220 nm) and the photoexcitation region (250 nm to 350 nm) two absorption regions,
21 ~~which result in suggest~~ different mechanisms for MIF formation, as discussed previously
22 (Whitehill and Ono, 2012; Ono et al., 2013; Whitehill et al., 2013).

23 In the 165 nm to 235 nm wavelength region, SO_2 photolysis occurs through predissociation
24 from the bound $\tilde{C}({}^1B_2)$ state. Near the dissociation threshold of 218.7 nm (Becker et al.,
25 1995), the quantum yield of photolysis is less than unity, although it increases to greater than
26 0.99 at wavelengths shorter than 215 nm (Katagiri et al., 1997). In the region where the
27 quantum yield is close to unity (i.e. less than 215 nm), the isotope effects due to SO_2
28 photolysis should be determined entirely by the differences in the absorption cross-sections
29 between the different isotopologues of SO_2 (e.g., by isotopologue specific Franck-Condon
30 coupling; Danielache et al., 2008) and optical screening effects under high SO_2 column

1 densities (Lyons, 2007, 2008; Ono et al., 2013). In the narrow spectral region from 215 nm to
2 218.7 nm, where the quantum yield of photodissociation varies, it is possible that quantum
3 yield differences between isotopologues could potentially produce additional isotope effects
4 beyond those predicted from absorption cross-sections. However, in this region,
5 photodissociation occurs primarily via vibronic mixing of the $\tilde{C}(^1B_2)$ state levels with the
6 dissociative continuum of the electronic ground, $\tilde{X}(^1A_1)$ state (Katagiri et al., 1997). Due to the
7 high density of vibronic levels for the $\tilde{X}(^1A_1)$ state, it is unlikely that there will be significant
8 isotope effects in the coupling strength between the $\tilde{C}(^1B_2)$ and $\tilde{X}(^1A_1)$ states. Dissociation
9 occurring through mixing with repulsive singlet and triplet states is expected to be small, as is
10 the nonadiabatic coupling of the $\tilde{C}(^1B_2)$ and $\tilde{D}(^1A_1)$ states (Tokue and Nanbu, 2010).

11 For laboratory experiments, the observed isotope effects for SO₂ photolysis is a function not
12 only of differences in the absorption cross-sections (Danielache et al., 2008) but also a
13 function of the SO₂ column density. This is because the SO₂ absorption cross-section has
14 significant fine structure, which causes optical screening effects to occur (Lyons, 2007). This
15 optical screening effect produces larger isotope effects at higher SO₂ column densities (Ono et
16 al., 2013). In addition to the above effects, there appears to be a total (or bath gas) pressure
17 effect on $\Delta^{33}\text{S}$ values. This manifests as reduced $\Delta^{33}\text{S}$ values at higher total (i.e. bath gas)
18 pressures, which is observed with He, SO₂, and N₂ bath gases (Masterson et al., 2011;
19 Whitehill and Ono, 2012; Ono et al., 2013). The mechanism responsible for these pressure
20 effects is still uncertain, but it could suggest that ³³SO₂ has a longer excited-state lifetime
21 prior to dissociation than the other isotopologues.

22 SO₂ photoexcitation in the 250 nm to 350 nm absorption region also produces absorption-based
23 isotope effects due to differences in cross-sections and self-shielding. In addition, it produces
24 isotope effects by a completely different mechanism. SO₂ photoexcitation in the 250 nm to
25 350 nm region occurs by initial excitation into a coupled $\tilde{A}(^1A_2)/\tilde{B}(^1B_1)$ singlet excited state
26 that undergoes intersystem crossing to the photochemically active triplet $\tilde{a}(^3B_1)$ state (Xie et
27 al., 2013; L  v  que et al., 2014). Unlike SO₂ photolysis, where the quantum yield of reaction
28 (i.e. photolysis) is near unity, the quantum yield for intersystem crossing between the singlet
29 and triplet states is highly variable and state-dependent. Due to the relatively low density of
30 states in the crossing region ($\tilde{A}(^1A_2) \rightarrow \tilde{a}(^3B_1)$), the branching between quenching to the ground
31 state and intersystem crossing to the triplet state will be a strong function of isotope
32 substitution. Whitehill et al. (2013) argue that this isotope selective intersystem crossing as

1 | the origin of ~~most-part~~ of the isotope effects in photochemical products following
2 | SO₂ photoexcitation in the 250 nm to 350 nm absorption region.

3 | Photoexcitation of SO₂ in the presence of O₂ produces sulfate with both positive $\Delta^{33}\text{S}$ and
4 | positive $\Delta^{36}\text{S}$ signals, similar to the organic sulfur observed in Whitehill et al. (2013) and the
5 | elemental sulfur in Whitehill and Ono (2012). This suggests that the anomalous isotope
6 | signatures observed from photoexcitation in previous studies are a result of the
7 | photophysics and photochemistry of excited-state SO₂ rather than the ~~photo~~chemistry of
8 | subsequent reactions (i.e., the chemistry with acetylene). Our experimental results show
9 | significant discrepancy with isotope effects predicted by isotopologue-specific absorption
10 | cross-sections (Danielache et al., 2012; Hattori et al., 2013) for the 250 nm to 320 nm region
11 | (Whitehill et al., 2013). This is expected if isotope selective intersystem crossing is
12 | ~~overprinting-contributing to~~ the isotope signals ~~produced-by-in addition to~~ cross section
13 | differences and shielding effects.

14 | **4.2 Temperature effects on SO₂ photolysis**

15 | Lyons (2007, 2008) presented isotopologue-specific absorption cross-sections for SO₂ in the
16 | 190 nm to 220 nm absorption region by shifting the measured ³²SO₂ absorption cross-sections
17 | of Freeman et al. (1984) by an amount based on the calculated isotope shifts of Ran et al.
18 | (2007). It has been unclear whether these absorption cross-sections can correctly predict the
19 | isotope effects due to SO₂ photolysis (Danielache et al. 2008), as they include only isotope
20 | shifts and not other potential differences among isotopologues. Previous comparisons with
21 | experimental data showed significant discrepancies (i.e. a factor of ~2 in $\delta^{34}\text{S}$ values) between
22 | experimental data and that predicted by the Lyons (2007, 2008) cross-sections (Whitehill and
23 | Ono, 2012; Ono et al., 2013). Such discrepancies were attributed to the difference in
24 | temperature between the Lyons (2007, 2008) cross-sections, which are based on cross-
25 | sections measured at 213 K (Freeman et al., 1984) and the temperature of the experiments
26 | (298 K). Given the new temperature data in the present study, it is possible to compare
27 | calculations based on the Lyons (2007, 2008) cross-sections with temperature-dependent
28 | experimental isotope data. Calculations were performed as described in previous papers
29 | (Whitehill and Ono, 2012; Ono et al., 2013) and are compared to experimental data in Figure
30 | 5.

1 Excellent agreement with the Lyons (2007,2008) cross-sections can be seen when the
2 observed temperature dependence on $\delta^{34}\text{S}$ are extrapolated back to 213 K. A similar strong
3 agreement is also seen in the $\Delta^{36}\text{S}$ values. This new data fills in the major gap between
4 predictions based on the Lyons (2007, 2008) cross-sections and the room-temperature
5 experimental data, and provides further support to an optical origin of mass-independent
6 fractionation during SO_2 photolysis under laboratory conditions (Ono et al., 2013).

7 Despite the strong agreement for $\delta^{34}\text{S}$ and $\Delta^{36}\text{S}$ values, the Lyons (2007, 2008) cross-sections
8 over-predict the magnitude of the mass-independent isotope anomaly in ^{33}S (i.e. $\Delta^{33}\text{S}$ values)
9 when compared with experimental data. There are several possible explanations for this. One
10 reason is that there are significant differences between the actual cross-sections and those
11 predicted by shifting the $^{32}\text{SO}_2$ cross-sections for $^{33}\text{SO}_2$. Measurements by Danielache et al.
12 (2008) at room temperature suggest that there are some differences between the isotopologue-
13 specific absorption cross-sections aside from just the spectral shifts accounted for by Lyons
14 (2007, 2008). A second possibility is that the high total pressure (101.3 kPa, including the N_2
15 bath gas) of the experiments caused a decrease in the $\Delta^{33}\text{S}$ value relative to values observed at
16 lower total pressures. It has been previously observed (Masterson et al., 2011; Whitehill and
17 Ono, 2012; Ono et al., 2013) that $\Delta^{33}\text{S}$ values decrease in the presence of high bath gas
18 pressures. This pressure quenching effect is most noticeable for $\Delta^{33}\text{S}$ and does not affect $\delta^{34}\text{S}$
19 or $\Delta^{36}\text{S}$ values as strongly.

20 The Lyons (2007, 2008) cross sections are semi-empirical in that they take the measured
21 $^{32}\text{SO}_2$ cross-sections of Freeman et al. (1984) and shift them using theoretical isotope shifts
22 predicted by Ran et al. (2007). Although the Lyons (2007, 2008) cross-sections are not
23 necessarily accurate.

24 ~~We that~~ the Lyons (2007, 2008) cross sections ~~seem to~~ accurately predict the isotope
25 effects during SO_2 photolysis under low temperature (ca. 213 K) conditions, such as those in
26 the stratosphere.

27 ~~Conversely, cross sections measured at room temperature (e.g., Danielache et al., 2008) will~~
28 ~~underestimate $\delta^{34}\text{S}$ fractionations when applied to stratospheric conditions.~~

29 **4.3 Constraining the rate of the $\text{SO} + \text{O}_2 + \text{M}$ reaction using product formation**

30 Our results demonstrate that photolysis of SO_2 in the presence of molecular oxygen (O_2)
31 produces large amounts of sulfate with considerable mass-independent sulfur isotope

1 anomalies. In our experimental system, there are three dominant pathways for SO₃
2 formation: OH oxidation of SO₂ (reactions R1 + R2, if water is present), O₂ oxidation of SO
3 from SO₂ photolysis (reactions R4 + R6), and O oxidation of SO₂ via



5 OH and O oxidation of SO₂ (reactions R1 and R7) are mass dependent (Harris et al., 2012;
6 Whitehill and Ono, 2012; Ono et al., 2013). However, oxidation of SO via R6 will trap the
7 isotopic composition of SO as SO₃ and carry the mass-independent sulfur isotope signature
8 from SO₂ photolysis (R4).

9 We performed a series of experiments at a total pressure of 101.3 kPa, a flow rate of 6.67 cm³
10 s⁻¹ (400 sccm) and an SO₂ partial pressure of 0.127 kPa (Table 4; Figure 6). The partial
11 pressure of molecular oxygen was varied from 0 kPa to 19.8 kPa (0 % to 19.5% O₂). In all
12 experiments, SO₂ was photolyzed via R4. In the experiments with no oxygen, both elemental
13 sulfur (S⁰) and SO₃ aerosols were formed, with the elemental sulfur (S and related species)
14 formed from SO via:



16 SO photolysis is expected to be a minor source of S compared to R8. In the absence of
17 oxygen, SO₃ is formed primarily via O oxidation of SO₂ (R7), which is mass dependent (Ono
18 et al., 2013).

19 At 5.1 kPa O₂ and above, elemental sulfur formation was shut off and SO₃ was the major
20 product. Under these conditions, oxidation of SO (to SO₂ or SO₃ via R5 or R6) competes
21 with SO disproportionation (R8).

22 By comparing the Δ³³S value of elemental sulfur in the absence of O₂ (0 kPa O₂) with the
23 Δ³³S value of sulfate in the presence of O₂ (5.1 kPa to 19.8 kPa O₂), it is possible to estimate
24 the fraction of sulfate formed through R6. In particular,

$$25 f_{\text{R6}} = \frac{\Delta^{33}\text{S}_{\text{sulfate, with O}_2}}{\Delta^{33}\text{S}_{\text{S}^0, \text{no O}_2}} \quad (5)$$

26 where f_{R6} is the fraction of total SO₃ formed that comes from reaction R6. Given the product
27 yields (Table 4), the time each experiment was run, and the volume of the reaction cell
28 (approximately 325 cm³), the sulfate formation rate per unit volume per unit time can be
29 calculated. In the experiments with 5.1 kPa to 19.8 kPa O₂, the sulfate formation rates were

1 between 5.3×10^{12} molecules $\text{cm}^{-3} \text{s}^{-1}$ and 1.2×10^{13} molecules $\text{cm}^{-3} \text{s}^{-1}$. Combining this with
 2 the f_{R6} values calculated from equation 5, we can estimate for the rate of sulfate formation
 3 from reaction R6 under our experimental conditions. This gave a rate for reaction 6 of
 4 3.6×10^{12} molecules $\text{cm}^{-3} \text{s}^{-1}$ to 6.6×10^{12} molecules $\text{cm}^{-3} \text{s}^{-1}$. Assuming R6 is a termolecular
 5 reaction, the rate for R6 can be written as:

$$6 \text{ rate R6} = k_{R6}[\text{SO}][\text{O}_2][\text{M}] \quad (6)$$

7 where k_{R6} is the termolecular rate constant for reaction R6 and $[\text{SO}]$, $[\text{O}_2]$ and $[\text{M}]$ are the
 8 concentrations of SO, O₂ and total third body gases ($\text{M} = \text{N}_2, \text{O}_2$) in the reaction cell. In
 9 equation (6), the $[\text{O}_2]$ and $[\text{M}]$ terms are known from the experimental conditions. The $[\text{SO}]$
 10 term is estimated by assuming a photochemical steady state for SO in the cell. SO production
 11 via Reaction R4 is balanced by SO destruction via Reactions R5 and R6. This gives us a
 12 steady state SO concentration of:

$$13 [\text{SO}] = \frac{J_{\text{SO}_2}[\text{SO}_2]}{k_{R5}[\text{O}_2] + k_{R6}[\text{O}_2][\text{M}]} \quad (7)$$

14 where J_{SO_2} is the photolysis rate constant for R4. This photolysis rate constant was calculated
 15 assuming a spectral irradiance for our 150 W Xe arc lamp of:

$$16 F_0 / \text{mW nm}^{-1} = 0.11 \cdot 1.6 \cdot (14 - 9 \cdot \exp(-0.013 \cdot (\lambda / \text{nm} - 200))) \quad (8)$$

17 where F_0 is the spectral irradiance of the xenon lamp at wavelength λ (Ono et al., 2013). This
 18 flux might be modified slightly as a function of the distance between the cell and the lamp,
 19 due to interferences from the absorption of oxygen. However, sensitivity studies performed
 20 here and previously (Whitehill and Ono, 2012) suggest that the effect of the oxygen
 21 absorption on the total SO₂ photolysis rate is minor compared to the uncertainty in the lamp
 22 photon flux. The lamp photon flux data was determined from the manufacturer's data and
 23 uncertainty estimates were not available. Despite this, the function used by Ono et al. (2013)
 24 (Equation 8) was used to obtain an estimate for the total SO₂ photolysis rate.

25 The spectral irradiance of the lamp was used to calculate the photon flux entering the cell,
 26 accounting for absorption of the cell windows from measured transmission data. The SO₂
 27 absorption cross-sections of Manatt and Lane (1993) were used to calculate the photolysis
 28 rate in the cell, accounting for optical screening effects from SO₂ and O₂ within the cell. With
 29 an SO₂ partial pressure of 0.127 kPa, this provided a photolysis rate constant of $J_{\text{SO}_2} = 5.2 \times 10^{-3}$
 30 s^{-1} . The rate constant for reaction R5 is $k_{R5} = 8.0 \times 10^{-17} \text{ cm}^3 \text{ molecule}^{-1} \text{ s}^{-1}$ (Sander et al.,

1 2011) at room temperature (298 K). Using these values and equations (6) and (7), the rate
2 constant for R6 (k_{R6}) was calculated iteratively. Calculated rate constants ranged from $k_{R6} =$
3 $7.3 \times 10^{-38} \text{ cm}^6 \text{ molecule}^{-2} \text{ s}^{-1}$ to $k_{R6} = 1.4 \times 10^{-37} \text{ cm}^6 \text{ molecule}^{-2} \text{ s}^{-1}$, with an average value of k_{R6}
4 $= 1.1 \times 10^{-37} \text{ cm}^6 \text{ molecule}^{-2} \text{ s}^{-1}$ (Table 4). This rate estimate is consistent with the upper bound
5 on $k_{R6} \leq 1 \times 10^{-36} \text{ cm}^6 \text{ molecule}^{-2} \text{ s}^{-1}$ by Black et al. (1982).

6 The calculated rate constant (k_{R6}) appears to decrease at 19.8 kPa O_2 compared with
7 the calculated rate for lower pO_2 values. It is unclear why this behavior is observed. The
8 relatively strong agreement for the other conditions strengthens our confidence that the model
9 is robust.

10 ~~The~~The derived rate constant carries a large amount of uncertainty due to a number of
11 sources of error in the rate calculation. One source of error in the calculation is in the spectral
12 irradiance of the xenon lamp, which was fit from the manufacturer's literature and not directly
13 measured. Because the spectral irradiance is likely to change over the lamp's lifetime, the
14 actual spectral irradiance at the time the experiments were performed might be different than
15 the values calculated here. As the spectral irradiance in the high-energy side of the ultraviolet
16 (190 nm to 220 nm) is likely to decrease over the course of the lamp's lifetime, this makes the
17 calculated SO_2 photolysis rate (and resulting SO number density) an upper bound. Reducing
18 the SO_2 photolysis rate increases the effective rate constant. A second source of error is the
19 assumption that we trapped 100% of the SO_3 formed as sulfate. It is possible that some
20 fraction of the SO_3 remained in the gas phase and did not condense as aerosol particles. A
21 third source of error is the assumption that the reaction R6 behaves as a termolecular reaction
22 despite the high total pressure (101.3 kPa) of the system. It is possible that the reaction is
23 saturated at (or near) this pressure and is thus behaving as an effective bimolecular reaction.
24 In any of these three cases, the estimate of the rate constant for reaction R6 would be a lower
25 bound on the actual termolecular rate constant.

26 It is also important to consider the impact of water vapor within the system. Although
27 attempts were made to minimize the amount of water vapor in the system, there was almost
28 certainly some water vapor in the system during our experiments. This is evidenced by
29 the visible formation of sulfate aerosols from SO_3 during the experiments. Unfortunately, we
30 did not have the analytical capability to quantitatively constrain the amount of water vapor in
31 the system during the experiments. The Zero Air and Nitrogen used as a source of gas to the
32 cell has a maximum of 3 ppm H_2O (by volume), but there could be additional water absorbed

Formatted: Indent: First line: 0.49"

1 onto the surfaces of the system while the cell is disassembled. We assume 100% of the SO₃
2 was trapped as sulfate, giving a lower bound estimate on the rate of reaction R6.

3 **4.4 Constraining the rate of the SO + O₂ + M reaction using a kinetic model**

4 To further constrain the rate of R6 (the SO + O₂ + M → SO₃ + M reaction), we constructed a
5 kinetic model of the chemistry occurring within the cell. We used the same data and
6 conditions as Section 4.3, but explicitly modeled the chemistry occurring within the system.
7 SO₂ photolysis rates were calculated as discussed in Section 4.3, using the cross sections of
8 Manatt and Lane (1993). Oxygen and ozone photolysis rates were calculated using the cross-
9 sections Yoshino et al. (1988, 1992) for O₂ and Molina and Molina(1986) for O₃. Quantum
10 yields for O(¹D) versus O(³P) formation from O₃ photolysis were parameterized based on the
11 recommendation of DeMore et al. (1997). Photolysis rates for HO₂ and H₂O₂ were calculated
12 using the recommended cross-sections of Sander et al. (2011). HO₂ photolysis was assumed
13 to produce O(¹D) and OH as products, and H₂O₂ photolysis was assumed to produce 2OH.-
14 O(¹D) formed from O₃ photolysis was assumed to be instantaneously quenched by N₂ and
15 O₂ to O(³P) and not significantly affect the chemistry of the system.

16 The rate constants and their sources~~Reactions considered, rate constants for those reactions,~~
17 and the sources for the rate constants are given in Table 9. ~~When possible, e~~Effective second-
18 order rate constants (calculated assuming T = 298 K and [M] = 2.5×10¹⁹ molecule cm⁻³) were
19 used for termolecular reactions. Initial guesses were made for the concentration of species
20 within the system. The system was assumed to be in photochemical steady state and solved
21 iteratively until convergence. Comparisons were made between the data and the calculations
22 for ~~both~~ f_{R6} values (Equation 5) ~~as well as total product (SO₃) formation rates.~~ Simulations
23 were performed with values of k_{R6} ~~between of~~ 1.0×10⁻³⁷ cm⁶ molecule⁻² s⁻¹, ~~and~~ 1.0×10⁻³⁶ cm⁶
24 molecule⁻² s⁻¹, and 1.0×10⁻³⁵ cm⁶ molecule⁻² s⁻¹. Since the amount of water vapor in the
25 system was not constrained experimentally, three simulations were performed, with H₂O
26 concentrations of 0 ppm (by volume), 10 ppm (by volume), and 100 ppm (by volume), which
27 spans a range of reasonable estimates for water vapor concentration in the system. Although
28 water vapor in the bath gas (N₂ and N₂/O₂) are less than 3 ppm (by volume), additional water
29 could be absorbed onto the inner surfaces of the cell and released during the
30 experiment. Results for 0 ppm H₂O and 10 ppm H₂O predict rates for reaction R6 on the order
31 of 10⁻³⁶ cm⁶ molecule⁻² s⁻¹, with predictions for 100 ppm H₂O being slightly higher.

1 There is a discrepancy between model predictions and the observed experimental behavior.
2 In particular, lower O₂ fractions produce higher estimated rates and vice versa. In addition, the
3 model predicts rates mostly higher than the previous upper bound on the rate calculated by
4 Black et al. (1982) of 10⁻³⁶ cm⁶ molecule⁻² s⁻¹. Helium was used as a bath gas for the Black et
5 al. (1982) experiments, as compared with nitrogen or nitrogen / oxygen used as the bath gas
6 here. Nitrogen (N₂) and oxygen (O₂) are a more efficient third body quenchers than helium.
7 Thus, the rate of the termolecular reaction with nitrogen (or nitrogen/oxygen) as a bath gas
8 could be higher than the maximum constraint suggested by Black et al. (1982). There is also
9 an order of magnitude discrepancy between the predictions here and those in Section 4.3, with
10 those in Section 4.3 being an order of magnitude smaller than those in Section 4.4. This could
11 be based on the assumption that 100% of the SO₃ was trapped as sulfate in Section 4.3,
12 whereas the actual amount might be less than that (implying a higher rate than predicted in
13 Section 4.3). However, the model predicts rate constants within an order of magnitude of
14 previous constraints from the literature (Black et al., 1982) and Section 4.3. Based on this
15 work, we estimate the rate of this reaction to be on the order of 10⁻³⁷ cm⁶ molecule⁻² s⁻¹ to 10⁻³⁶
16 cm⁶ molecule⁻² s⁻¹. Future work is necessary to better constrain the rate of this reaction.

17 The observed k_{R6} value (equation 5) is best fit by the k_{R6} between 2×10^{-37} cm⁶ molecule⁻²
18 s⁻¹ and 10×10^{-37} cm⁶ molecule⁻² s⁻¹ (Figure 7, left). The yield of SO₃ indicates a lower
19 rate constant of less than 1×10^{-37} cm⁶ molecule⁻² s⁻¹ to 3×10^{-37} cm⁶ molecule⁻² s⁻¹,
20 potentially reflecting low recovery of SO₃ in our experiments (Figure 7, right). Nonetheless,
21 this range of results is consistent with the rate estimate obtained in Section 4.3. Thus, our best
22 estimate for the rate of reaction R6 is somewhere between 1.0×10^{-37} cm⁶ molecule⁻² s⁻¹ and
23 1.0×10^{-36} cm⁶ molecule⁻² s⁻¹. As discussed in Section 4.3, the model is sensitive to the SO₂
24 photolysis rate, which depends upon the lamp spectrum.

25 4.5 Exploring the potential energy surfaces of the SO + O₂ reactions

26 The experimental evidence presented above suggests the formation of SO₃ via the SO+O₂
27 reaction. Our theoretical analysis shows that the singlet PES is associated with the ground
28 state of the SO₃ molecule, and thus is the primary surface related to the SO(³Σ⁻) + O₂(³Σ_g⁻)
29 →SO₃(¹A₁) reaction (Figure 4). As shown in Table 7, four isomers of SO₃ are located in the
30 singlet PES. It is predicted that the D_{3h}SO₃ molecule isomer is the global minimum, followed
31 by the cyclic-OSOO. There are two shallower wells, denoted as trans-OSOO and cis-OSOO,

Formatted: Subscript

Formatted: Superscript

Formatted: Superscript

Formatted: Superscript

Formatted: Superscript

Formatted: Not Superscript/ Subscript

Formatted: Not Superscript/ Subscript

Formatted: Not Superscript/ Subscript

Formatted: Not Superscript/ Subscript

Formatted: Not Superscript/ Subscript

Formatted: Not Superscript/ Subscript

Formatted: Not Superscript/ Subscript

Formatted: Not Superscript/ Subscript

Formatted: Not Superscript/ Subscript

Formatted: Not Superscript/ Subscript

Formatted: Not Superscript/ Subscript

Formatted: Not Superscript/ Subscript

Formatted: Not Superscript/ Subscript

Formatted: Not Superscript/ Subscript

Formatted: Not Superscript/ Subscript

Formatted: Not Superscript/ Subscript

Formatted: Not Superscript/ Subscript

Formatted: Not Superscript/ Subscript

Formatted: Not Superscript/ Subscript

Formatted: Not Superscript/ Subscript

Formatted: Subscript

1 | at the CASPT2 and UCCSD(T)-F12a levels, but they [seem appear](#) to be energetically higher
2 | than the $\text{SO}({}^3\Sigma^-) + \text{O}_2({}^3\Sigma_g^-)$ asymptote at the B3LYP and CASSCF levels. No barrier was
3 | found for the formation of either trans-OSOO or cis-OSOO, but there is a barrier for the
4 | isomerization and the barrier height depends upon the level of the ab-initio calculation. The
5 | rate-determining barrier for the $\text{SO}({}^3\Sigma^-) + \text{O}_2({}^3\Sigma_g^-) \rightarrow \text{SO}_3({}^1\text{A}_1')$ reaction is the one connecting
6 | ~~the~~ cyclic-OSOO and SO_3 . The lowest barrier height for this reaction (given by CASPT2) is
7 | $56.6 \text{ kJ mole}^{-1}$. Using the partition function at the B3LYP level, a conventional transition-
8 | state theory rate calculation predicts a pressure-saturated (i.e. effective bimolecular) thermal
9 | rate constant for reaction R6 at 298K of $2.7 \times 10^{-24} \text{ cm}^3 \text{ molecule}^{-1} \text{ s}^{-1}$. This is about eight
10 | orders of magnitude lower than the experimental rate constant for reaction R5 ($8.0 \times 10^{-17} \text{ cm}^3$
11 | $\text{molecule}^{-1} \text{ s}^{-1}$, Sander et al., 2011), and about six orders of magnitude lower than the
12 | minimum effective second-order rate constant for reaction R6 at 101.3 kPa total pressure
13 | (about $2.5 \times 10^{-18} \text{ cm}^3 \text{ molecule}^{-1} \text{ s}^{-1}$, calculated assuming $k_{\text{R6}} = 1.0 \times 10^{-37} \text{ cm}^6 \text{ molecule}^{-1} \text{ s}^{-1}$ and
14 | $[\text{M}] = 2.5 \times 10^{19}$). We thus conclude that the $\text{SO}({}^3\Sigma^-) + \text{O}_2({}^3\Sigma_g^-) \rightarrow \text{SO}_2({}^1\text{A}_1) + \text{O}({}^3\text{P})$ reaction
15 | cannot occur on the singlet surface without invoking the spin-forbidden intersystem crossing
16 | between the singlet and triplet surfaces.

17 | The triplet PES is very different from the singlet PES with regard to the energy of each SO_3
18 | isomer (Figure 4; Table 8). The global minimum moves to the cyclic-OSOO [isomer](#), which
19 | has a similar geometry to the singlet (ground) state counterpart but with different bond
20 | lengths. On the other hand, $\text{SO}_3({}^3\text{A}_1')$ becomes highly unfavorable; for example, it is 75.14 kJ
21 | mole^{-1} higher than the $\text{SO} + \text{O}_2$ reactants at the UCCSD(T)-F12a level. The trans-OSOO
22 | complex remains in a planar geometry, in which the O-S-O-O dihedral angle is 180° ;
23 | however, the cis-OSOO complex was found to be out-of-plane, in which the O-S-O-O
24 | dihedral angle is about 74° . We still use “cis-OSOO” to denote this isomer for convenience.
25 | Unlike the singlet PES, trans-OSOO and cis-OSOO share the same transition state for the
26 | isomerization to cyclic-OSOO. This process represents the rate-limiting step for the reaction
27 | on the triplet surface. The barrier height is $67.86 \text{ kJ mole}^{-1}$ at the UCCSD(T)-F12a level,
28 | which is still high. In the adiabatic picture, the $\text{SO}({}^3\Sigma^-) + \text{O}_2({}^3\Sigma_g^-) \rightarrow \text{SO}_2({}^1\text{A}_1) + \text{O}({}^3\text{P})$
29 | reaction on the triplet PES has a rate constant of $2.7 \times 10^{-25} \text{ cm}^3 \text{ molecule}^{-1} \text{ s}^{-1}$ at 298 K,
30 | estimated using transition-state theory. This is still considerably slower than the
31 | experimentally measured rate constant for reaction R5.

1 It is clear that a single PES is unable to reproduce the experimental data for reactions R5 and
2 R6. ~~The deviation is rather large and cannot be attributed to tunneling effects.~~ In order to
3 explore the possibility of intersystem crossing, two adiabatic minimum energy pathways on
4 both spin states are shown in Figure 4 and the energies are extracted at the UCCSD(T)-
5 F12a//B3LYP level. There are several places that the two PESs cross each other, and a spin
6 flip could happen in the region near the cyclic-OSOO isomer due to the fact that ~~this cyclic-~~
7 ~~OSOO~~-isomer on both PESs has nearly the same energy. A possible non-adiabatic reaction
8 pathway is depicted in Figure 4 by the green solid lines connecting every two stationary
9 points. Specifically, for the $\text{SO}({}^3\Sigma^-) + \text{O}_2({}^3\Sigma_g^-) \rightarrow \text{SO}_3({}^1\text{A}_1')$ reaction, the two reactants first
10 approach each other to form cyclic-OSOO on the singlet PES, and jump to the triplet PES to
11 avoid the high barrier region, followed by back transition to the singlet state to form the SO_3
12 product. For the $\text{SO}({}^3\Sigma^-) + \text{O}_2({}^3\Sigma_g^-) \rightarrow \text{SO}_2({}^1\text{A}_1) + \text{O}({}^3\text{P})$ reaction, the intermediate cyclic-
13 OSOO may be generated on the singlet PES, followed by intersystem crossing from the
14 singlet to triplet surface and then reach the products without overcoming a high barrier.
15 Indeed, several different mechanisms introduce the intersystem crossing have been
16 proposed by other authors for the $\text{SO}_3 \rightarrow \text{SO}_2 + \text{O}$ reactions (Davis, 1974; Westenberg and
17 Dehaas, 1975; Astholz et al., 1979), thanks to the relatively large spin-orbit coupling of the
18 heavy sulfur. The barrier associated with the intersystem crossing pathway seems to be
19 consistent with the fast rate of R5, and supports the facile formation of SO_3 .

20 Unfortunately, rate constants involving the intersystem crossing cannot be readily determined
21 ~~from the current calculations, without a~~ global PESs for both spin states and the coupling
22 between them would be required for a complete calculation. Such a goal can only be
23 achieved by a multi-reference method or configuration interaction method, which is infeasible
24 at the current level. ~~On-the-fly transition state surface hopping calculations would present an~~
25 alternative method to derive rate constants without the need for global potential energy
26 surfaces and should be pursued in future work.

27 **4.6 Contribution of the $\text{SO} + \text{O}_2 + \text{M}$ reaction to sulfate formation in the** 28 **stratosphere**

29 To determine the significance of the reaction R6 to sulfate formation in the stratosphere, we
30 compared the rate of sulfate formation via R6 to that formed via OH oxidation of SO_2
31 (reaction R1) and O oxidation of SO_2 (reaction R7) under a select set of atmospheric

1 conditions. We assumed an atmospheric temperature and pressure profile of the U.S. Standard
 2 Atmosphere 1976 (COESA, 1976) and noon-time O, OH, and O₃ concentrations given by
 3 DeMore et al. (1997). Spectral photon flux in the 180 nm to 220 nm region was calculated as
 4 a function of altitude for a solar zenith angle of 40° by assuming the spectral photon irradiance
 5 of Rottman et al. (2006) at the top of the atmosphere and O₂, O₃, and CO₂ being the dominant
 6 absorbers. Absorption cross-sections of O₂ (Yoshino et al., 1988, 1992), O₃ (Molina and
 7 Molina, 1986), and CO₂ (Shemansky, 1972) were used with concentration and column density
 8 data for the species to calculate the transmission of the atmosphere to radiation in the 180 nm
 9 to 220 nm absorption region at different altitudes. SO₂ photolysis rate constants (J_{SO_2}) were
 10 calculated as a function of altitude using the calculated spectral photon fluxes and the SO₂
 11 absorption cross-sections of Manatt and Lane (1993).

12 The lifetime of SO with respect to oxidation by O₂ (i.e. R5 and R6) is relatively short (on the
 13 order of seconds), so SO and SO₂ were assumed to be in photochemical steady state, i.e.

$$14 \quad \frac{[SO]}{[SO_2]} = \frac{J_{SO_2}}{k_{R5}[O_2] + k_{R6}[O_2][M]} \quad (9)$$

15 The rate constant k_{R5} was calculated as a function of altitude (i.e. temperature) based on the
 16 recommendations of Sander et al. (2011). k_{R6} was varied between $1.0 \times 10^{-37} \text{ cm}^6 \text{ molecule}^{-2} \text{ s}^{-1}$
 17 ¹ and $1.0 \times 10^{-36} \text{ cm}^6 \text{ molecule}^{-2} \text{ s}^{-1}$ to encompass ~~our range of the order of magnitude~~
 18 estimates from Section 4.3 and 4.4. SO oxidation by other oxidants (O₃, O, NO₃, etc.) was
 19 assumed to be minor compared to oxidation by O₂ given the minor concentration of most of
 20 these species compared with that of O₂. Using the [SO] to [SO₂] ratio, the rates of R1, R7,
 21 and R6 can be compared. Assuming these three reactions are the dominant source of SO₃
 22 (and subsequently sulfate) in the stratosphere, the fraction of sulfate from reaction R6 (f_{SO})
 23 can be calculated as:

$$24 \quad f_{SO} = \frac{\frac{[SO]}{[SO_2]} \cdot k_{R6}[O_2][M]}{k_{SO_2+OH}[OH] + k_{SO_2+O}[O] + \frac{[SO]}{[SO_2]} \cdot k_{R6}[O_2][M]} \quad (10)$$

25 The rate constants k_{SO_2+OH} and k_{SO_2+O} are the effective bimolecular rate constants for reactions
 26 R1 and R7, as recommended by Sander et al. (2011). f_{SO} values were calculated for a 40°
 27 solar zenith angle (local noon at 40°N latitude and a 0° solar declination angle) and are shown
 28 in Figure 8. Given that SO, OH, and O(³P) are all formed as a result of photochemistry, they

1 should have similar daily cycles. As a result, the f_{SO} values calculated for local noon should
2 be similar to daily average f_{SO} values.

3 | As seen in Figure 8, the lower-bound estimate for k_{R6} (1.0×10^{-37} cm⁶ molecule⁻² s⁻¹) gives 4%
4 to 10% of sulfate from R6 between 25 km and 50 km altitude. A faster estimate for k_{R6} of
5 2.0×10^{-37} cm⁶ molecule⁻² s⁻¹ gives 8% to 18% of sulfate from R6 between 25 km and 50 km
6 altitude. The upper bound estimate for the rate ($k_{R6} = 1.0 \times 10^{-36}$ cm⁶ molecule⁻² s⁻¹, from
7 Black et al., 1982) suggests that over 45% of sulfate could be coming from R6 between 31 km
8 and 34 km altitude and is probably unrealistic. The contribution from R6 depends upon the
9 amount of photons available for SO₂ photolysis, which increases with altitude because of less
10 absorption by Schuman-Runge band of O₂ and the Hartley bands of O₃. The rate of R6
11 decreases at higher altitude as total number density decrease. The maximum f_{SO} value, thus,
12 is between 30 and 35 km (Figure 8).

13 Some insight into the rate can be obtained from SO₂ lifetimes in the stratosphere. Following
14 the Mt. Pinatubo (1991) eruption, the Total Ozone Mapping Spectrometer (TOMS) data
15 (Bluth et al., 1992) and Microwave Limb Sounder (MLS) data (Read et al., 1993) were used
16 to estimate an e-folding time of 33 days to 35 days for SO₂ in the stratosphere. A later
17 reanalysis of the TOMS data and TIROS Optical Vertical Sounder (TOVS) data (Guo et al.,
18 2004) reduced this value to 25 days. Bekki and Pyle (1994) modeled the SO₂ decay following
19 the Mt. Pinatubo eruption, considering R1 as the only sink of SO₂ in the stratosphere. Their
20 modeled decay times for SO₂ (40 days) are considerably longer than the measured value of 25
21 days. Bekki and Pyle (1994) attributed this to uncertainties in the OH number densities. The
22 discrepancy, however, could be explained in part by SO₂ photolysis followed by R6. Inclusion
23 | of the SO₂ photolysis sink would decrease the lifetimes for SO₂ above around 25 km. The
24 presence of this reaction would also suggest that OH concentrations estimated by Read et al.
25 | (1993) based on SO₂ lifetimes might overestimate OH concentrations above around 25 km
26 altitude.

27 SO₂ photolysis is self-limiting, as SO₂ photolysis near the top of the volcanic SO₂ plume
28 absorbs ultraviolet radiation in the range that SO₂ photolysis occurs. As a result, SO₂
29 photolysis lower in the eruption cloud is reduced and depends upon the overlying SO₂ column
30 density. This would potentially reduce the significance of R6 under heavy SO₂ loading.

31 Optical shielding effects increase the magnitude of the isotope effect from SO₂ photolysis
32 under high SO₂ column densities (Lyons et al., 2007; Ono et al., 2013). Thus, the isotope

1 fractionation occurring in a volcanic cloud is a tradeoff between larger fractionations but
2 lower photolysis rates at higher column densities versus smaller fractionations but higher
3 photolysis rates at lower column densities. Although the instantaneous fractionation factors
4 can be ~~accurately~~ estimated using our results and cross section by Lyons (2007, 2008), the
5 temporal evolution of isotope signatures of sulfate aerosol will require a model that accurately
6 incorporates both chemistry and dynamics of stratosphere.

7 Given the large signal produced by SO₂ photolysis, over 100‰ and 10‰ for δ³⁴S and Δ³³S
8 values, respectively (Whitehill and Ono, 2012; Ono et al., 2013), even a 10% contribution
9 from reaction R5 could make a substantial contribution to the isotope signature of sulfate
10 formed above circa 25 km altitude. Given the strong similarity in the isotopic signature of
11 stratospheric sulfate aerosols from volcanic eruptions and those produced during SO₂
12 photolysis (Figure 3), it is likely that SO₂ photolysis plays an important role in the sulfur
13 isotope budget of stratospheric sulfate aerosols. The initial sulfate formed from SO₂
14 photolysis (followed by R6) will contain positive δ³⁴S and Δ³³S values and negative Δ³⁶S
15 values. Over time, due to mass balance, the residual SO₂ will obtain negative δ³⁴S and Δ³³S
16 values and positive Δ³⁶S values. This explains the temporal evolution of the isotopic
17 signatures observed in aerosol samples (for δ³⁴S, Castleman et al., 1974) and ice cores (Baroni
18 et al., 2007), which goes from positive δ³⁴S and Δ³³S values shortly after an eruption to
19 negative values as time progresses.

20

21 **4.7 Insignificance of excited-state photochemistry of SO₂ in the stratosphere**

22 It has been suggested previously (Savarino et al., 2003; Hattori et al., 2013) that excited-state
23 photochemistry of SO₂ in the 250 nm to 350 nm absorption region (i.e. the $\tilde{A}(^1A_2)/\tilde{B}(^1B_1)$
24 states) might be ~~important-the dominant source of~~ the sulfur isotope ratios in stratospheric
25 sulfate aerosols. Previous results (Whitehill and Ono, 2012; Whitehill et al., 2013) have
26 demonstrated that SO₂ photoexcitation in this region produces mass-independent sulfur
27 isotope signatures with positive Δ³⁶S/Δ³³S ratios, as opposed to the negative Δ³⁶S/Δ³³S ratios
28 measured for stratospheric sulfate aerosols. This study further demonstrates that
29 SO₂ photoexcitation in the 250 nm to 350 nm absorption region produces positive Δ³⁶S/Δ³³S
30 ratios, even at temperatures approaching stratospheric temperatures. Our previous
31 experiments (Whitehill and Ono, 2012; Whitehill et al., 2013) have been questioned as being

1 inapplicable to the modern atmosphere (Hattori et al., 2013) due to the experimental
2 conditions (i.e. the addition of C₂H₂ to trap triplet-state SO₂). In the present study, we tested
3 SO₂ photoexcitation with two different longpass filters (250 nm longpass filter and 280 nm
4 longpass filter) in a N₂/O₂ bath gas. In all cases, we produced sulfate products with positive
5 $\Delta^{36}\text{S}/\Delta^{33}\text{S}$ ratios. Therefore, our experiments do not provide support for SO₂ photoexcitation
6 as a the dominant source of the isotope anomalies in modern atmospheric samples.

7 However, contribution from both absorption bands to the isotope effects observed in
8 stratospheric sulfate aerosols is possible and should be considered further. Despite the strong
9 correspondence between $\Delta^{36}\text{S}/\Delta^{33}\text{S}$ ratios in our photolysis experiments and stratospheric
10 sulfate aerosol samples (Figure 3), the stratospheric sulfate aerosol samples produces a
11 slightly shallower (less negative) $\Delta^{36}\text{S}/\Delta^{33}\text{S}$ slope than the majority of our experimental
12 samples. This could be due in part to the effect of pressure on $\Delta^{36}\text{S}/\Delta^{33}\text{S}$ ratios (Masterson et
13 al., 2011), as the one experiment performed at 7.7 kPa total pressure (Table 5) produced a
14 $\Delta^{36}\text{S}/\Delta^{33}\text{S}$ more similar to the stratospheric sulfate aerosol samples than the experiments
15 performed at 101.3 kPa total pressure. It could also be due, however, to mixing between the
16 negative $\Delta^{36}\text{S}/\Delta^{33}\text{S}$ signatures from SO₂ photolysis and the positive $\Delta^{36}\text{S}/\Delta^{33}\text{S}$ signatures from
17 SO₂ photoexcitation. It is critical that future experiments further explore the isotope effects
18 within these two absorption regions. However, it is also clear that SO₂ photoexcitation alone
19 is not likely to be responsible for the isotope signatures and that SO₂ photolysis is necessary
20 as well.

21 **4.8 Caveats for Experimental Studies**

22 There are a number of difficulties with directly applying photochemical results from
23 laboratory studies to processes occurring in the natural environment. One issue is the
24 difference between the spectral photon flux of the Xe and D₂ arc lamps as compared with the
25 solar spectrum. Comparisons of data from different light sources (Xe versus D₂ lamps) were
26 made previously in static photochemical experiments (Whitehill and Ono, 2012) and showed
27 minor differences depending upon the light source. However, despite the large differences in
28 the spectral photon flux between the Xe and D₂ light sources, the patterns in the isotope
29 fractionation (i.e. $\delta^{34}\text{S}$ versus $\Delta^{33}\text{S}$ versus $\Delta^{36}\text{S}$) are similar. Both the Xe and D₂ light sources
30 are broadband, unstructured light sources in the 180 nm to 220 nm absorption region, where
31 SO₂ photolysis occurs. The solar spectrum, although also broadband, has considerably more
32 fine structure in the spectrum, due to absorption by other gases such as O₂. As demonstrated

Formatted: Normal, Indent: First line: 0.4"

1 in early SO₂ photolysis experiments (Farquhar et al. 2001), highly structured light sources
2 (such as laser light sources) can cause anomalous isotope effects different from those
3 observed in a broadband regime (Whitehill and Ono, 2012).

4 Unfortunately, the currently available measured absorption cross-sections (Danielache
5 et al. 2008) do not reproduce the results of photochemical experiments (Whitehill and Ono,
6 2012). As shown by Ueno et al. (2009), they predict negative $\Delta^{33}\text{S}$ values from SO₂
7 photolysis under reasonable atmospheric conditions. Photochemical experiments show
8 positive $\Delta^{33}\text{S}$ values near zero (except in the self-shielding regime; Ono et al., 2013) under
9 similar conditions. It is also important to note that the magnitude of uncertainties in the cross-
10 section measurements (on the percent level) are too large to be considered quantitative for that
11 of mass-independent fractionation observed in these reactions. Future, higher-precision and
12 higher resolution cross-section measurements should resolve some of these discrepancies and
13 allow for stratospheric fractionations under solar spectral conditions to be modeled. In the
14 absence of this data, however, experiments using solar-like spectra (i.e. Xe arc lamp) can
15 provide a first order constraint on the types of isotope fractionations expected under a solar
16 regime.

17 Another major issue with the experiments that was discussed above is the poor control
18 in the experiments over the amount of water in the system. Due to the fact that experiments
19 were performed at room temperature rather than at vacuum, it is difficult to put definitive
20 constraints on the amount of water present in the system. Although attempts were made to
21 flush the systems with nitrogen (< 3 ppb H₂O) prior to each experiment, water could be
22 adsorbed onto the surfaces of the system. The presence of water will cause HO_x chemistry to
23 occur and open up an additional (mass-dependent, Harris et al. 2012) channel for sulfate
24 formation. The amount of water in the system also affects the amount of SO₃ that ends up as
25 sulfate aerosols. This is particularly an issue when attempting to estimate the rate of reactions
26 in the system (Section 4.3 and 4.4). Differences in the amount of water within the system
27 during different experiments could explain some of the isotopic variability between replicate
28 experiments (Tables 4 and 5). Photoexcitation (250 nm to 350 nm) experiments performed in
29 an identical photochemical system but with the addition of acetylene (C₂H₂) are not strongly
30 affected by the presence of trace amounts of water in the system, and showed considerably
31 better isotopic reproducibility (Whitehill et al. 2013; Table 3) than SO₂ photolysis
32 experiments (Ono et al., 2013; Tables 2, 4, and 5). This suggests that variability in trace

Formatted: Subscript

Formatted: Subscript

1 amounts of water present in the system could have a significant affect on the isotopic
2 signatures during SO₂ photolysis, and that water vapor should be carefully controlled in future
3 experiments.
4

5 **4.84.9 Production and preservation of mass-independent sulfur isotope** 6 **signatures in ice cores**

7 The results presented in this paper can explain the production and preservation of mass-
8 independent sulfur isotope signatures in the modern atmosphere. Large volcanic eruptions,
9 such as Pinatubo (1991) and Agung (1963) inject large amounts of SO₂ into the stratosphere.
10 Both direct injection into higher altitudes (i.e. above around 20 to 25 km) or stratospheric
11 transport of the SO₂ plume can bring SO₂ to a sufficient altitude for SO₂ photolysis to occur.
12 The process of SO₂ photolysis produces large mass-independent sulfur isotope signatures in
13 the SO products, particularly when there is high SO₂ loading (and thus optical screening
14 effects). Reaction of SO with O₂ to produce SO₃ (via R6) provides a pathway for the isotopic
15 signature of SO to be preserved as SO₃, which can subsequently form sulfate aerosols. Some
16 portion of the sulfate aerosols containing the mass-independent sulfur isotope signatures are
17 transported to polar regions, where they can be deposited in polar precipitation and preserved
18 in ice core records. A schematic illustration of the process is shown in Figure 9.

19 Some eruptions, despite their stratospheric influence, produce sulfate peaks in ice core records
20 but do not contain mass-independent sulfur isotope signatures. Such eruptions include Cerro
21 Hudson (1991, Savarino et al., 2003) and Laki (1783, Lanciki et al., 2012). Schmidt et al.
22 (2012) discussed this issue previously and concluded that the Laki aerosols deposited in the
23 Greenland ice cores were predominantly upper tropospheric or lower stratospheric in
24 origin. Estimates for the height of the Laki (1783) eruption plume are only 15 km (Thordarson
25 and Self, 2003), which penetrates the stratosphere but is not sufficiently high for SO₂
26 photolysis to be a dominant process (Schmidt et al., 2012). Due to the higher latitude of the
27 eruption, transport processes are unlikely to bring the eruption plume to a sufficient altitude
28 (25 km) for SO₂ photolysis to occur. Thus, despite the stratospheric influence of the Laki
29 eruption, mass-independent sulfur isotope signatures in the preserved aerosols would not be
30 expected. The situation is similar for the Cerro Hudson (1991) eruption, which had an
31 injection height of 11 km to 16 km (Schoeberl et al., 1993). Again, given the high latitude of

1 | the eruption, transport processes are likely insufficient to bring the plume ~~above 25 km to a~~
2 | ~~sufficient altitude for SO₂ photolysis to become a dominant process.~~
3 | ~~In contrast with this are major low~~Low-latitude eruptions such as Pinatubo (1991) ~~might~~
4 | ~~behave differently.~~ Although the initial injection of the Pinatubo eruption was probably
5 | localized below 25 km, the evolution of the plume resulted in the plume reaching altitudes of
6 | 30 km or higher (Gobi et al., 1992), sufficient altitudes for SO₂ photolysis to play a role in the
7 | oxidation to sulfate. The largest mass-independent sulfur isotope signatures (with $\Delta^{33}\text{S} >$
8 | 1‰) observed to date are from the Samalas (1257, Lavigne et al., 2013) eruption (Lanciki et
9 | al., 2012). Evidence suggests the eruption plume from this reaction reached a minimum of 34
10 | km altitude, with a likely estimate being 43 km altitude (Lavigne et al., 2013). At this
11 | altitude, SO₂ photolysis would become a dominant process, and could explain why the
12 | signature from this eruption is significantly larger than the other eruptions. Thus, SO₂
13 | photolysis, followed by SO oxidation to SO₃ (via R6), presents a consistent mechanism
14 | through which mass-independent sulfur isotope signatures can be produced and preserved in
15 | the modern, oxygenated stratosphere.

16

17 | 5 Conclusions

18 | Laboratory photochemical experiments were carried ~~out~~ to investigate the production of
19 | mass-independent sulfur isotope effects under stratospheric conditions. For SO₂ photolysis in
20 | the 190 nm to 220 nm region, the magnitude of the mass-independent isotope signature
21 | increases with decreasing temperature. The isotope systematics, in particular $\delta^{34}\text{S}$ and $\Delta^{36}\text{S}$
22 | values, show excellent agreement with an optical self-screening model based on synthetic
23 | absorption cross sections (Lyons, 2007). SO₂ photoexcitation experiments show similar
24 | signatures to previous experimental studies (Whitehill and Ono, 2012; Whitehill et al., 2013),
25 | with positive $\Delta^{33}\text{S}$ and $\Delta^{36}\text{S}$ values, but that differ significantly from expectations based on
26 | absorption cross sections (Danielache et al., 2012).

27 | The SO₃ (recovered as sulfate) products from SO₂ photolysis in the presence of molecular
28 | oxygen carry mass-independent sulfur isotope signatures, suggesting a pathway for the direct
29 | oxidation of SO to SO₃. We hypothesize the SO + O₂ + M → SO₃ + M reaction (R6) and
30 | estimate the termolecular rate constant of the reaction to be on the order of 10⁻³⁷ cm⁶

1 | molecules⁻² s⁻¹ or faster. This is consistent with previous constraints on the maximum rate of
2 | this reaction (Black et al., 1982).

3 | We calculated the energies of stationary points on the singlet and triplet potential energy
4 | surfaces of SO₃ that are associated with the SO(³Σ⁻)+O₂(³Σ_g⁻) asymptote at several different
5 | levels of theory and show that reaction R6 is theoretically possible via intersystem crossing
6 | between the singlet and triplet surfaces. We also show that the measured rate for SO + O₂ +
7 | → SO₂ + O reaction (R5) also requires intersystem crossing between the singlet and triplet
8 | surfaces.

9 | Depending on the rate of R6, we predict that on the order of 10% of sulfate above 25 km
10 | altitude could be derived from the SO + O₂ + M channel. Given the large isotope
11 | fractionations produced during SO₂ photolysis, our model can explain the source and
12 | preservation mechanism of mass-independent sulfur isotope signatures measured in
13 | stratospheric sulfate aerosols in polar ice samples. Furthermore, oOur model explains the
14 | temporal evolution of δ³⁴S and Δ³³S values following major volcanic eruptions, and constrains
15 | the maximum altitude of the plume to above 20 to 25 km ~~and above~~ when non-zero Δ³³S values
16 | are observed.

17 | **Acknowledgements**

18 | The authors would like to thank William J. Olszewski for his assistance in sulfur isotope
19 | analysis, and support from NASA Exobiology (NNX10AR85G to S.O., and 11-EXO11-0107
20 | to H.G.) and NSF FESD (Award 1338810 to S.O.). The authors would like to thank editor
21 | Thomas Röckmann and reviewers Matthew Johnson and Joel Savarino for their comments.
22 |

1 **References**

- 2 Ahmed, M. M.: Theoretical studies on the ground and excited states of SO₃ triatomic
3 molecule, *Chem. Sci. Trans.*, 2, 781-796, doi: 10.7598/cst2013.515, 2013.
- 4 Astholz, D. C., Glanzer, K., and Troe, J.: The spin-forbidden dissociation-recombination
5 reaction SO₃→ SO₂+O, *J. Chem. Phys.*, 70, 2409-2413, doi:10.1063/1.437751, 1979.
- 6 Baroni, M., Thiemens, M. H., Delmas, R. J., and Savarino, J.: Mass-independent sulfur
7 isotopic compositions in stratospheric volcanic eruptions, *Science*, 315, 84-87
8 doi:10.1126/science.1131754, 2007.
- 9 Baroni, M., Savarino, J., Cole-Dai, J., Rai, V. K., and Thiemens, M. H.: Anomalous sulfur
10 isotope compositions of volcanic sulfate over the last millennium in Antarctic ice cores, *J.*
11 *Geophys. Res. Atmos.*, 113, D20112, doi:10.1029/2008JD010185, 2008.
- 12 Becke, A. D., Density-functional exchange-energy approximation with correct asymptotic
13 behavior, *Phys. Rev. A.*, 38, 3098-3100, doi:10.1103/PhysRevA.38.3098, 1988.
- 14 Becker, S., Braatz, C., Lindner, J., and Tiemann, E.: Investigation of the predissociation of
15 SO₂: state selective detection of the SO and O fragments, *Chem. Phys.*, 196, 275-291,
16 doi:10.1016/0301-0104(95)00114-4, 1995.
- 17 Bekki, S: Oxidation of volcanic SO₂: a sink for stratospheric OH and H₂O, *Geophys. Res.*
18 *Lett.*, 22, 913-916, doi:10.1029/95GL00534, 1995.
- 19 Bekki, S. and Pyle, J. A.: A two-dimensional modeling study of the volcanic eruption of
20 Mount Pinatubo, *J. Geophys. Res.*, 99, 18861-18869, doi:10.1029/94JD00667, 1994.
- 21 Black, G., Sharpless, R. L., and Slanger, T. G.: Rate coefficients at 298 K for SO reactions
22 with O₂, O₃, and NO₂, *Chem. Phys. Lett.*, 90, 55-58, doi:10.1016/0009-2614(82)83324-1,
23 1982.
- 24 Bluth, G. J. S., Doiron, S. D., Schnetzler, C. C., Krueger, A. J., and Walter, L. S.: Global
25 tracking of the SO₂ clouds from the June, 1991 Mount Pinatubo eruptions, *Geophys. Res.*
26 *Lett.*, 19, 151-154, doi: 10.1029/91GL02792, 1992.
- 27 Canfield, D. E., Raiswell, R., Westrich, J. T., Reaves, C. M., and Berner, R. A.: The use of
28 chromium reduction in the analysis of reduced inorganic sulfur in sediments and shales,
29 *Chem. Geol.*, 54, 149-155, doi:10.1016/0009-2541(86)90078-1, 1986.

1 Castleman, A. W., Munkelwitz, H. R., and Manowitz, B.: Isotopic studies of the sulfur
2 component of the stratospheric aerosol layer, *Tellus*, 26, 222-234, doi:10.1111/j.2153-
3 3490.1974.tb01970.x, 1974.

4 Celani, P. and Werner H.-J.: Multireference perturbation theory for large restricted and
5 selected active space reference wave functions, *J. Chem. Phys.*, 112, 5546-5557,doi:
6 10.1063/1.481132, 2000.

7 Cobos, C. J., Hippler, H., and Troe, J.: Falloff curves of the recombination reaction $O + SO +$
8 $M \rightarrow SO_2 + M$ in a variety of bath gases, *J. Phys. Chem.*, 89, 1778-1783, doi:
9 10.1021/j100255a048, 1985.

10 COESA (Committee on Extension to the Standard Atmosphere): U.S. Standard Atmosphere,
11 1976, U. S. Government Printing Office, Washington, D. C., United States of America, 1976.

12 Chase, M. W., Davies, C. A., Downey, J. R., Frurip, D. J., McDonald, R. A., and Syverud, A.
13 N.: NIST JANAF THERMOCHEMICAL TABLES 1985 Version 1.0, Standard Reference
14 Data Program, National Institute of Standards and Technology, Gaithersburg, MD,
15 <http://kinetics.nist.gov/janaf/>, 1986.

16 Chung, K., Calvert, J. G., and Bottenheim, J. W.: The photochemistry of sulfur dioxide
17 excited within its first allowed band (3130 Å) and the “forbidden” band (3700-4000 Å), *Int. J.*
18 *Chem. Kinet.*, 7, 161-182, doi: 10.1002/kin.550070202, 1975.

19 Danielache, S. O., Eskebjerg, C., Johnson, M. S., Ueno, Y., and Yoshida, N.: High-precision
20 spectroscopy of ^{32}S , ^{33}S , and ^{34}S sulfur dioxide: ultraviolet absorption cross sections and
21 isotope effects, *J. Geophys. Res. Atmos.*, 113, D17314, doi:10.1029/2007JD009695, 2008.

22 Danielache, S. O., Hattori, S., Johnson, M. S., Ueno, Y., Nanbu, S., and Yoshida,
23 N.:Photoabsorption cross-section measurements of ^{32}S , ^{33}S , ^{34}S , and ^{36}S sulfur dioxide for the
24 $B^1B_1-X^1A_1$ absorption band, *J. Geophys. Res. Atmos.*, 117, D24301,
25 doi:10.1029/2012JD017464, 2012.

26 Davis, D. D.: A kinetics review of atmospheric reactions involving H_xO_y compounds, *Can. J.*
27 *Chem.*, 52, 1405-1414,doi: 10.1139/v74-213, 1974.

28 DeMore, W. B., Sander, S. P., Golden, D. M., Hampson, R. F., Kurylo, M. J., Howard, C. J.,
29 Ravishankara, A. R., Kolb, C. E., and Molina, M. J.: Chemical kinetics and photochemical

1 data for use in stratospheric modeling, evaluation number 12, JPL Publication 97-4, Jet
2 Propulsion Laboratory, Pasadena, California, USA, 1997.

3 Dunning, T. H.: Gaussian basis sets for use in correlated molecular calculations. I. The atoms
4 boron through neon and hydrogen, *J. Chem. Phys.*, 90, 1007-1023, doi:
5 10.1063/1.456153,1989.

6 Forrest, J. and Newman, L.: Silver-110 microgram sulfate analysis for the short time
7 resolution of ambient levels of sulfur aerosol, *Anal. Chem.*, 49, 1579-1584,
8 doi:10.1021/ac50019a030, 1977.

9 Freeman, D. E., Yoshino, K., Esmond, J. R., and Parkinson, W. H., High resolution
10 absorption cross section measurements of SO₂ at 213 K in the wavelength region 172-240 nm,
11 *Planet. Space Sci.*, 32, 1125-1134, doi: 10.1016/0032-0633(84)90139-9, 1984.

12 Frisch, M. J., Trucks, G. W., Schlegel, H. B., Scuseria, G. E., Robb, M. A., Cheeseman, J. R.,
13 Scalmani, G., Barone, V., Mennucci, B., Petersson, G. A., Nakatsuji, H., Caricato, M., Li, X.,
14 Hratchian, H. P., Izmaylov, A. F., Bloino, J., Zheng, G., Sonnenberg, J. L., Hada, M., Ehara,
15 M., Toyota, K., Fukuda, R., Hasegawa, J., Ishida, M., Nakajima, T., Honda, Y., Kitao, O.,
16 Nakai, H., Vreven, T., Montgomery, J. A., Jr.; Peralta, J. E., Ogliaro, F., Bearpark, M., Heyd,
17 J. J., Brothers, E., Kudin, K. N., Staroverov, V. N., Kobayashi, R., Normand, J., Raghavachari,
18 K., Rendell, A., Burant, J. C., Iyengar, S. S., Tomasi, J., Cossi, M., Rega, N., Millam, M. J.,
19 Klene, M., Knox, J. E., Cross, J. B., Bakken, V., Adamo, C., Jaramillo, J., Gomperts,
20 R., Stratmann, R. E., Yazyev, O., Austin, A. J., Cammi, R., Pomelli, C., Ochterski, J. W.,
21 Martin, R. L., Morokuma, K., Zakrzewski, V. G., Voth, G. A., Salvador, P., Dannenberg, J. J.,
22 Dapprich, S., Daniels, A. D., Farkas, Ö., Foresman, J. B., Ortiz, J. V., Cioslowski, J., Fox, D.
23 J.: Gaussian 09, Gaussian, Inc., Wallingford, CT, <http://www.gaussian.com/>, 2009.

24 Gobbi, G. P., Congeduti, F., and Adriani, A.: Early stratospheric effects of the Pinatubo
25 eruption, *Geophys. Res. Lett.*, 19, 997-1000, doi:10.1029/92GL01038, 1992.

26 Goodarzi, M., Vahedpour, M., and Nazari, F.: Theoretical study on the atmospheric formation
27 of SO_x ($x = 1 - 3$) in the SSO(¹A') and O₂(³Σ_g⁻) reaction, *J. Molec. Struct. THEOCHEM*, 945,
28 45-52, doi: 10.1016/j.theochem.2010.01.004, 2010.

29 Guo, S., Bluth, G. J. S., Rose, W. I., Watson, I. M., Prata, A. J.: Re-evaluation of SO₂ release
30 of the 15 June 1991 Pinatubo eruption using ultraviolet and infrared satellite sensors,
31 *Geochem. Geophys. Geosyst.*, 5, Q04001, doi:10.1029/2003GC000654, 2004.

1 Harris, E., Sinha, B., Hoppe, P., Crowley, J. N., Ono, S., and Foley, S.: Sulfur isotope
2 fractionation during oxidation of sulfur dioxide: gas-phase oxidation by OH radicals and
3 aqueous oxidation by H₂O₂, O₃, and iron catalysis, *Atmos. Chem. Phys.*, 12, 407-424,
4 doi:10.5194/acp-12-407-2012, 2012.

5 Harris, E., Sinha, B., Hoppe, P., and Ono, S.: High-precision measurements of ³³S and ³⁴S
6 fractionation during SO₂ oxidation reveal causes of seasonality in SO₂ and sulfate isotopic
7 composition, *Environ. Sci. Tech.*, 47, 12174-12183, doi: 10.1021/es402824c, 2013.

8 Hattori, S., Schmidt, J., Johnson, M. S., Danielache, S. O., Yamada, A., Ueno, Y., and
9 Yoshida, N.: SO₂ photoexcitation mechanism links mass-independent sulfur isotopic
10 fractionation in cryospheric sulfate to climate impacting volcanism, *Proc. Natl. Acad. Sci.*
11 *USA*, 110, 17656-17661, doi:10.1073/pnas.1213153110, 2013.

12 Jou, S. H., Shen, M. Y., Yu, C. H., and Lee, Y. P.: Isomers of SO₃: infrared absorption of
13 OSOO in solid argon, *J. Chem. Phys.*, 104, 5745-5753, doi:10.1063/1.471335, 1996.

14 Katagiri, H., Sako, T., Hishikawa, A., Yazaki, T., Onda, K., Yamanouchi, K., and Yoshino,
15 K.: Experimental and theoretical exploration of photodissociation of SO₂ via the C¹B₂ state:
16 identification of the dissociation pathway, *J. Molec. Struct.*, 413-414, 589-614, doi:
17 10.1016/S0022-2860(97)00199-3, 1997.

18 Knizia, G., Adler, T. B., and Werner, H.-J.: Simplified CCSD(T)-F12 methods: theory and
19 benchmarks, *J. Chem. Phys.*, 130, 054104, doi: 10.1063/1.3054300, 2009.

20 Knowles, P. J. and Werner, H.-J.: An efficient second-order MC SCF method for long
21 configuration expansions, *Chem. Phys. Lett.*, 115, 259-267, doi: 10.1016/0009-
22 2614(85)80025-7, 1985.

23 Knowles, P. J. and Werner, H.-J.: An efficient method for the evaluation of coupling
24 coefficients in configuration interaction calculations, *Chem. Phys. Lett.*, 145, 514-522, doi:
25 10.1016/0009-2614(88)87412-8, 1988.

26 Lanciki, A. L.: Discovery of sulfur mass-independent fractionation (MIF) anomaly of
27 stratospheric volcanic eruptions in Greenland ice cores, Ph.D. thesis, South Dakota State
28 University, Brookings, South Dakota, United States of America, 141 pp., 2010.

1 Lanciki, A., Cole-Dai, J., Thiemens, M. H., and Savarino, J.: Sulfur isotope evidence of little
2 or no stratospheric impact by the 1783 Laki volcanic eruption, *Geophys. Res. Lett.*, 39,
3 L01806, doi:10.1029/2011GL050075, 2012.

4 Lavigne, F., Degeai, J. P., Komorowski, J. C., Guillet, S., Robert, V., Lahitte, P.,
5 Oppenheimer, C., Stoffel, M., Vidal, C. M., Surono, Pratomo, I., Wassmer, P., Hajdas, I.,
6 Hadmoko, D. S., and Belizal, E.: Source of the great A.D. 1257 mystery eruption unveiled,
7 Samalas volcano, Rinjani Volcanic Complex, Indonesia, *Proc. Natl. Acad. Sci. USA (Early*
8 *Edition)*,doi: 10.1073/pnas.1307520110, 2013.

9 Lee, C., Yang, W., and Parr, R. G., Development of the Colle-Salvetti correlation-energy
10 formula into a functional of electron density, *Phys. Rev. B.*, 37, 785-789, doi:
11 10.1103/PhysRevB.37.785,1988.

12 Leung, F., Colussi, A. J., and Hoffmann, M. R.: Sulfur isotopic fractionation in the gas-phase
13 oxidation of sulfur dioxide initiated by hydroxyl radicals, *J. Phys. Chem. A*, 105, 8073-8076,
14 doi:10.1021/jp011014+, 2001.

15 Lévêque, C., Taïeb, R., and Köppel, H.: Communication: theoretical prediction of the
16 importance of the 3B_2 state in the dynamics of sulfur dioxide, *J. Chem. Phys.*, 140, 091101
17 doi:10.1063/1.4867252, 2014.

18 Lyons, J. R.: Mass-independent fractionation of sulfur isotopes by isotope-selective
19 photodissociation of SO₂, *Geophys. Res. Lett.*, 34, L22811, doi:10.1029/2007GL031031,
20 2007.

21 Lyons, J. R.: Photolysis of long-lived predissociative molecules as a source of mass-
22 independent isotope fractionation: the example of SO₂, *Adv. Quant. Chem.*, 55, 57-74, doi:
23 10.1016/S0065-3276(07)00205-5, 2008.

24 Manatt, S. L. and Lane, A. L.: A compilation of the absorption cross-sections of SO₂ from
25 106 to 403 nm, *J. Quant. Spectrosc. Radiat. Transfer*, 50, 267 - 276, doi:10.1016/0022-
26 4073(93)90077-U, 1993.

27 Martin, J. M. L.: Heat of atomization of sulfur trioxide, SO₃: a benchmark for computational
28 thermochemistry, *Chem. Phys. Lett.*, 310, 271-276,doi: 10.1016/S0009-2614(99)00749-6,
29 1999.

1 Masterson, A. L., Farquhar, J., and Wing, B. A.: Sulfur mass-independent fractionation
2 patterns in the broadband UV photolysis of sulfur dioxide: pressure and third body effects,
3 Earth Planet. Sci. Lett., 306, 253-260, doi:10.1016/j.epsl.2011.04.004, 2011.

4 Molina, L. T. and Molina, M. J.: Absolute absorption cross sections of ozone in the 185- to
5 350-nm wavelength range, J. Geophys. Res. Atmos., 91, 14501-14501, doi:
6 10.1029/JD091iD13p14501, 1986.

7 Oduro, H., Kamyshny Jr, A., Guo, W., and Farquhar, J.: Multiple sulfur isotope analysis of
8 volatile organic sulfur compounds and their sulfonium precursors in coastal marine
9 environments, Marine Chem., 124, 78-89, doi:10.1016/j.marchem.2010.12.004, 2011.

10 Ono, S., Whitehill, A. R., and Lyons, J. R.: Contribution of isotopologue self-shielding to
11 sulfur mass-independent fractionation during sulfur dioxide photolysis, J. Geophys. Res.
12 Atmos., 118, 2444-2454, doi:10.1002/jgrd.50183, 2013.

13 [Pavlov, A. A. and Kasting, J. F.: Mass-independent fractionation of sulfur isotopes in
14 Archean sediments: Strong evidence for an anoxic Archean atmosphere. *Astrobiology*, 2, 27–
15 41, doi:10.1089/153110702753621321, 2002.](#)

16 Pavlov, A. A., Mills, M. J., and Toon, O. B.: Mystery of the volcanic mass-independent sulfur
17 isotope fractionation signature in the Antarctic ice core, Geophys. Res. Lett., 32, L12816,
18 doi:10.1029/2005GL022784, 2005.

19 [Phillips, L. F.: Absolute absorption cross sections for SO between 190 and 235 nm. *J. Phys.*
20 *Chem.*, 85, 3994 – 4000, doi: 10.1021/j150626a009, 1981.](#)

21 Ran, H., Xie, D., and Guo, H.: Theoretical studies of the C¹B₂ absorption spectra of
22 SO₂ isotopomers, Chem. Phys. Lett., 439, 280-283, doi: 10.1016/j.cplett.2007.03.103, 2007.

23 Read, W. G., Froidevaux, L., and Waters, J. W.: Microwave limb sounder measurement of
24 stratospheric SO₂ from the Mt. Pinatubo Volcano, Geophys. Res. Lett., 20, 1299-1302, doi:
25 10.1029/93GL00831, 1993.

26 Robock, A.: Volcanic eruptions and climate, Rev. Geophys., 38(2), 191-219,
27 doi:10.1029/1998RG000054, 2000.

28 Rottman, G. J., Woods, T. N., and McClintock, W.: SORCE solar UV irradiance results, Adv.
29 Space Res., 37, 201-208, doi: 10.1016/j.asr.2005.02.072, 2006.

1 Sander, S. P., Abbatt, J., Barker, J. R., Burkholder, J. B., Friedl, R. R., Golden, D. M., Huie,
2 R. E., Kolb, C. E., Kurylo, M. J., Moortgat, G. K., Orkin, V. L., and Wine, P. H.: Chemical
3 kinetics and photochemical data for use in atmospheric studies, evaluation no. 17, JPL
4 Publication 10-6, Jet Propulsion Laboratory, Pasadena, California, USA,
5 <http://jpldataeval.jpl.nasa.gov/>, 2011.

6 Savarino, J., Romero, J., Cole-Dai, J., Bekki, S., and Thiemens, M. H.: UV induced mass-
7 independent sulfur isotope fractionation in stratospheric volcanic sulfate, *Geophys. Res. Lett.*,
8 30, 2131, doi:10.1029/2003GL018134, 2003.

9 Schmidt, A., Thordarson, T., Oman, L. D., Robock, A., and Self, S.: Climatic impact of the
10 long-lasting 1783 Laki eruption: inapplicability of mass-independent sulfur isotopic
11 composition measurements, *J. Geophys. Res.*, 117, D23116, doi: 10.1029/2012JD018414,
12 2012.

13 Schoeberl, M. R., Doiron, S. D., Lait, L. R., Newman, P. A., and Krueger, A. J.: A simulation
14 of the Cerro Hudson SO₂ cloud, *J. Geophys. Res.*, 98, 2949-2955, doi:10.1029/92JD02517,
15 1993.

16 Shemansky, D. E.: CO₂ extinction coefficient 1700-3000A, *J. Chem. Phys.*, 56, 1582, doi:
17 10.1063/1.1677408, 1972.

18 Tanaka, N., Rye, D. M., Xiao, Y., and Lasaga, A. C.: Use of stable sulfur isotope systematics
19 for evaluating oxidation reaction pathways and in-cloud scavenging of sulfur-dioxide in the
20 atmosphere, *Geophys. Res. Lett.*, 21, 1519–1522, doi:10.1029/94GL00893, 1994.

21 Thordarson, T. and Self, S.: Atmospheric and environmental effects of the 1783-1784 Laki
22 eruption: a review and reassessment, *J. Geophys. Res.*, 108, 4011,
23 doi:10.1029/2001JD002042, 2003.

24 Tokue, I. and Nanbu, S.: Theoretical studies of absorption cross sections for the C¹B₂-X¹A₁
25 system of sulfur dioxide and isotope effects, *J. Chm. Phys.*, 132, 024301, doi:
26 10.1063/1.3277191, 2010.

27 [Tsang, W. and Hampson, R. F.: Chemical kinetic database for combustion chemistry. Part I.](#)
28 [Methane and related compounds. *J. Phys. Chem. Ref. Data*, 15, 1087 – 1279.](#)
29 [doi:10.1063/1.555759, 1986.](#)

1 Werner, H.-J., Knowles, P. J., Knizia, G., Manby, F. R., Schütz, M., Celani, P., Korona, T.,
2 Lindh, R., Mitrushenkov, A., Rauhut, G., Shamasundar, K. R., Adler, T. B., Amos, R. D.,
3 Bernhardsson, A., Berning, A., Cooper, D. L., Deegan, M. J. O., Dobbyn, A. J., Eckert, F., Goll,
4 E., Hampel, C., Hesselmann, A., Hetzer, G., Hrenar, T., Jansen, G., Köppl, C., Liu, Y., Lloyd,
5 A. W., Mata, R. A., May, A. J., McNicholas, S. J., Meyer, W., Mura, M. E., Nicklass, A.,
6 O'Neill, D. P., Palmieri, P., Peng, D., Pflüger, K., Pitzer, R., Reiher, M., Shiozaki, T., Stoll, H.,
7 Stone, A. J., Tarroni, R., Thorsteinsson, T., and Wang, M.: MOLPRO, version 2012.1, a
8 package of ab initio programs, Cardiff, UK, <http://www.molpro.net>, 2012.

9 Westenberg, A. A. and Dehaas, N.: Rate of the O + SO₃ reaction, *J. Chem. Phys.*, 62, 725-
10 730, doi: 10.1063/1.430477, 1975.

11 Whitehill, A. R., and Ono, S.: Excitation band dependence of sulfur isotope mass-independent
12 fractionation during photochemistry of sulfur dioxide using broadband light sources,
13 *Geochim. Cosmochim. Acta*, 94, 238-253, doi:10.1016/j.gca.2012.06.014, 2012.

14 Whitehill, A. R., Xie, C., Hu, X., Xie, D., Guo, H., and Ono, S.: Vibronic origin of sulfur
15 mass-independent isotope effect in photoexcitation of SO₂ at the implications to the early
16 earth's atmosphere, *Proc. Natl. Acad. Sci. USA*, 110, 17697-17702,
17 doi:10.1073/pnas.1306979110, 2013.

18 Xie, C., Hu, X., Zhou, L., Xie, D., and Guo, H.: *Ab initio* determination of potential energy
19 surfaces for the first two UV absorption bands of SO₂, *J. Chem. Phys.*, 139, 014305, doi:
20 10.1063/1.4811840, 2013.

21 Yoshino, K., Cheung, A. S. C., Esmond, J. R., Parkinson, W. H., Freeman, D. E., Guberman,
22 S. L., Jenouvrier, A., Coquart, B., and Merienne, M. F.: Improved absorption cross-sections
23 of oxygen in the wavelength region 205-240 nm of the Herzberg continuum, *Planet. Space*
24 *Sci.*, 36, 1469-1475, doi: 10.1016/0032-0633(88)90012-8, 1988.

25 Yoshino, K., Esmond, J. R., Cheung, A. S. C., Freeman, D. E., and Parkinson, W. H.: High
26 resolution absorption cross sections in the transmission window of the Schumann-Runge
27 bands and Herzberg continuum of O₂, *Planet. Space Sci.*, 40, 185-192, doi: 10.1016/0032-
28 0633(92)90056-T, 1992.

29

1 Table 1. Summary of experiments performed

Experiment	Lamp	Filter	T / K	Bath Gas	Presented in
photolysis (temp.)	200 W D ₂	None	225 to 275	N ₂	Figures 2, 5; Table 2
photoexcitation (temp.)	150 W Xe	250 LP, H ₂ O	225 to 275	N ₂ /C ₂ H ₂	Figure 2; Table 3
photolysis (added O ₂)	150 W Xe	None, 200 BP	298	N ₂ /O ₂	Figures 3, 6; Tables 4, 5
photoexcitation (added O ₂)	150 W Xe	250 LP, 280 LP	298	N ₂ /O ₂	Figure 3; Table 5

2

1 Table 2. Isotope ratios of elemental sulfur products from the SO₂ photolysis temperature
2 experiments (Section 2.2)

<i>T</i> / K	$\delta^{33}\text{S}$ / ‰	$\delta^{34}\text{S}$ / ‰	$\delta^{36}\text{S}$ / ‰	$\Delta^{33}\text{S}$ / ‰	$\Delta^{36}\text{S}$ / ‰
225	103.05	191.16	349.12	8.02	-32.4
225	97.85	177.76	315.71	9.13	-35.8
250	87.19	161.31	288.97	6.61	-29.8
250	80.68	146.58	259.31	7.18	-28.9
275	72.16	132.59	236.37	5.57	-24.1
275	70.35	129.04	227.26	5.50	-25.5

3

1 Table 3. Isotope ratios of organosulfur products from the SO₂photoexcitation temperature
2 experiments (Section 2.2)

<i>T</i> / K	$\delta^{33}\text{S}$ / ‰	$\delta^{34}\text{S}$ / ‰	$\delta^{36}\text{S}$ / ‰	$\Delta^{33}\text{S}$ / ‰	$\Delta^{36}\text{S}$ / ‰
225	24.18	9.88	65.72	19.01	46.0
225	24.94	9.95	67.09	19.73	47.2
250	25.29	7.33	64.39	21.44	49.7
250	24.30	6.37	62.38	20.96	49.6
275	26.24	5.39	63.29	23.4	52.5
275	25.39	4.84	61.27	22.84	51.6

3

4

1 Table 4. Results from experiments of SO₂ photolysis in the presence of varying amounts of O₂
 2 (Section 2.3) used to estimate k_{R6} (Sections 4.3 and 4.4).

Product	$pO_2 /$ kPa	Time / ks	Yield / $\mu\text{mol S}$	$\delta^{33}\text{S} /$ ‰	$\delta^{34}\text{S} /$ ‰	$\delta^{36}\text{S} /$ ‰	$\Delta^{33}\text{S} /$ ‰	$\Delta^{36}\text{S} /$ ‰	calculated $k_{R6} /$ $\text{cm}^6 \text{ molecule}^{-2} \text{ s}^{-1}$
*S ⁰ - 1	0.00	21.6		74.00	129.68	220.54	8.63	-31.9	
*S ⁰ - 2	0.00	21.6		78.42	137.52	232.90	9.18	-34.8	
S ⁰ avg	0.00						8.91	-33.3	
*SO ₃ - 1	0.00	21.6	35.3	14.16	25.64	43.82	1.02	-5.2	
*SO ₃ - 2	0.00	21.6	28.9	11.51	21.14	36.21	0.67	-4.2	
SO ₃	5.07	7.2	46.0	45.47	79.75	134.34	4.97	-19.5	1.4×10^{-37}
SO ₃	5.07	7.2	32.6	50.85	89.24	150.93	5.59	-21.6	1.1×10^{-37}
SO ₃	10.13	7.2	37.1	51.60	90.27	151.99	5.82	-22.5	1.3×10^{-37}
SO ₃	10.13	7.2	41.3	51.35	91.22	155.00	5.13	-21.5	1.3×10^{-37}
SO ₃	15.20	7.2	37.4	51.43	89.67	150.68	5.94	-22.6	1.3×10^{-37}
SO ₃	15.20	7.2	20.8	55.14	97.09	164.55	5.97	-23.4	7.3×10^{-38}
SO ₃	19.75	10.8	40.4	53.18	94.68	161.22	5.24	-22.2	8.3×10^{-38}
SO ₃	19.75	10.8	39.1	54.18	96.59	164.45	5.29	-22.7	8.1×10^{-38}

3 * S⁰ - 1 and SO₃ - 1 are elemental sulfur and SO₃ from the same experiment. Similarly, S⁰ - 2
 4 and SO₃ - 2 are elemental sulfur and SO₃ from the same experiment.

5

6

1 Table 5. Results from additional experiments of SO₂ photolysis in the presence of O₂ (Section
 2 2.3). All results are from sulfate (SO₃) product. Experiments were performed at a constant
 3 total pressure of 101.3 kPa unless marked otherwise. Filter types are: 200 BP = 200 nm
 4 bandpass filter, 250 LP = 250 nm longpass filter, 280 LP = 280 nm longpass filter.

Filter	p_{SO_2} / Pa	p_{O_2} / kPa	Flow / $\text{cm}^3 \text{ s}^{-1}$	Time / ks	Yield / $\mu\text{mol S}$	$\delta^{33}\text{S}$ / ‰	$\delta^{34}\text{S}$ / ‰	$\delta^{36}\text{S}$ / ‰	$\Delta^{33}\text{S}$ / ‰	$\Delta^{36}\text{S}$ / ‰
none	314.0	19.00	16.67	1.8	62.3	38.45	67.23	117.84	4.22	-12.2
none	316.6	18.99	6.67	12.8	105.7	34.71	60.89	104.88	3.69	-12.5
none	50.7	20.06	1.67	18.0	70.9	32.91	58.18	95.36	3.26	-16.2
none	50.7	20.06	1.67	10.8	41.8	37.46	67.09	112.12	3.34	-17.0
none	25.2	20.16	1.68	18.0	40.8	22.80	40.08	64.63	2.31	-12.0
none	25.2	20.16	1.68	10.8	19.3	19.59	35.15	58.01	1.61	-9.2
*none	349.9	0.20	0.29	19.8	34.0	34.02	59.04	104.90	3.92	-9.2
200 BP	316.6	18.99	6.67	67.8	86.2	47.67	89.15	162.21	2.59	-11.9
200 BP	50.7	20.06	1.67	36.0	-	35.65	65.22	111.79	2.50	-14.0
250 LP	506.5	18.23	1.67	61.2	14.9	9.40	15.97	32.53	1.19	1.9
250 LP	506.5	18.23	1.67	61.2	1.9	19.56	33.12	68.70	2.60	4.5
280 LP	316.6	18.99	6.67	86.4	6.7	3.22	4.25	9.34	1.03	1.2

5 * Experiment performed at 7.7 kPa total pressure to test low pressure limit

1 Table 6. Comparison of asymptotic energies of SO+O₂ obtained on the singlet and triplet
 2 potential energy surfaces for SO₃ and those obtained by the sum of two separated species. All
 3 energies are in kJ mole⁻¹ and are relative to the SO(³Σ⁻) + O₂(³Σ_g⁻) calculated separately in
 4 each ab-initio method.

	B3LYP	CASSCF	CASPT2//CASSCF	UCCSD(T)F12a//B3LYP
SO(³ Σ ⁻) + O ₂ (³ Σ _g ⁻)	0	0	0	0
(separated)				
SO(¹ Δ) + O ₂ (³ Σ _g ⁻)				
(separated)	118.78	64.60	136.36	94.98
SO(³ Σ ⁻) + O ₂ (¹ Δ _g)				
(separated)	160.83	86.57	98.28	121.55
SO(¹ Δ) + O ₂ (¹ Δ _g)				
(separated)	279.57	151.17	234.64	216.48
SO+O ₂ (singlet)	279.57	0.00	-6.86	217.19
SO+O ₂ (triplet)	27.61	0.00	-6.61	122.59

5
6

1 Table 7. Energies for stationary points on the singlet state potential energy surface at various
 2 ab-initio levels. The energy is relative to the $\text{SO}(^3\Sigma^-) + \text{O}_2(^3\Sigma_g^-)$ asymptote and zero point
 3 energy is not included. All energies are given in kJ mole^{-1} .

	B3LYP	CASSCF	CASPT2//CASSCF	UCCSD(T)F12a//B3LYP
SO_3	-287.73	-262.92	-348.69	-411.58
cyclic-OSOO	-60.17	-50.21	-101.75	-142.72
trans-OSOO	42.09	53.72	-18.87	-17.66
cis-OSOO	19.33	35.82	-31.42	-39.08
TS1: trans-to-cis	108.95	135.14	66.32	42.76
TS2: trans-to-cyclic	62.51	69.71	3.10	0.17
TS3: cis-to-cyclic	108.95	114.18	50.42	43.26
TS4: cyclic-to- SO_3	82.42	69.25	56.61	70.33
$\text{SO}(^3\Sigma^-) + \text{O}_2(^3\Sigma_g^-)$	0.00	0.00	0.00	0.00
$\text{SO}_2(^1\text{A}_1) + \text{O}(^1\text{D})$	292.04	159.28	206.27	152.84

4

5

1 Table 8. Energies for stationary points on the triplet state potential energy surface at various
 2 ab-initio levels. The energy is relative to the $\text{SO}({}^3\Sigma^-) + \text{O}_2({}^3\Sigma_g^-)$ asymptote and zero point
 3 energy is not included. All energies are given in kJ mole^{-1} .

	B3LYP	CASSCF	CASPT2//CASSCF	UCCSD(T)F12a//B3LYP
SO_3	136.02	293.21	115.90	75.14
cyclic-OSOO	-70.67	12.18	-105.06	-137.07
trans-OSOO	26.40	85.81	8.70	16.53
cis-OSOO	28.58	82.09	16.82	18.49
TS1: trans-to-cis	30.42	92.72	10.79	25.44
TS2: OSOO-to- cyclic	96.40	125.35	67.28	67.86
$\text{SO}_2 \dots \text{O}$	23.35	-71.34	-31.55	-58.28
TS3: cyclic-to- $\text{SO}_2 \dots \text{O}$	25.44	-62.93	-24.81	-54.06
$\text{SO}({}^3\Sigma^-) + \text{O}_2({}^3\Sigma_g^-)$	0.00	0.00	0.00	0.00
$\text{SO}_2({}^1\text{A}_1) + \text{O}({}^3\text{P})$	26.69	-55.44	13.64	-52.93

4
5

1 Table 9. Reactions and rate constants included in the kinetic model of the chemistry occurring
 2 within reaction cell. Rate constants have units of s^{-1} for first order reactions, $cm^3 molecule^{-1} s^{-1}$
 3 1 for second order reactions (and effective second order reactions, denoted *2), and cm^6
 4 $molecule^{-2} s^{-1}$ for third order reactions.

Reaction Number	Reaction	Rate constant	Reaction Order	Source
<u>Photochemical Reactions</u>				
1	$O_2 + h\nu \rightarrow O + O$	1.0×10^{-5}	1	Yoshino et al. (1988, 1992)
2	$O_3 + h\nu \rightarrow O + O_2$	5.7×10^{-3}	1	Molina and Molina (1986)
3	$O_3 + h\nu \rightarrow O(^1D) + O_2$	1.0×10^{-1}	1	Molina and Molina (1986)
4	$H_2O_2 + h\nu \rightarrow OH + OH$	1.7×10^{-3}	1	Sander et al. (2011)
5	$HO_2 + h\nu \rightarrow O(^1D) + OH$	1.5×10^{-2}	1	Sander et al. (2011)
6	$SO_2 + h\nu \rightarrow SO + O$	5.2×10^{-3}	1	Manatt and Lane (1993)
7	$SO + h\nu \rightarrow S + O$	9.7×10^{-3}	1	Phillips (1981)
<u>O₂ Chemistry</u>				
8	$O + O + M \rightarrow O_2 + M$	2.5×10^{-14}	*2	Tsang and Hampson (1986)
9	$O + O_2 + M \rightarrow O_3 + M$	1.5×10^{-14}	*2	Sander et al. (2011)
10	$O + O_3 \rightarrow O_2 + O_2$	8.0×10^{-15}	2	Sander et al. (2011)
<u>O(^1D) Chemistry</u>				
11	$O(^1D) + O_2 \rightarrow O + O_2$	4.0×10^{-11}	2	Sander et al. (2011)
12	$O(^1D) + O_3 \rightarrow O_2 + O_2$	1.2×10^{-10}	2	Sander et al. (2011)
13	$O(^1D) + O_3 \rightarrow O + O + O_2$	1.2×10^{-10}	2	Sander et al. (2011)
14	$O(^1D) + H_2 \rightarrow OH + H$	1.2×10^{-10}	2	Sander et al. (2011)
15	$O(^1D) + H_2O \rightarrow OH + OH$	2.0×10^{-10}	2	Sander et al. (2011)
16	$O(^1D) + N_2 \rightarrow O + N_2$	3.1×10^{-11}	2	Sander et al. (2011)
17	$O(^1D) + SO_2 \rightarrow ?$	2.2×10^{-10}	2	Sander et al. (2011)
<u>HO₂ Chemistry</u>				
18	$O + OH \rightarrow O_2 + H$	3.3×10^{-11}	2	Sander et al. (2011)

- Formatted ... [1]
- Formatted ... [2]
- Formatted ... [4]
- Formatted ... [5]
- Formatted ... [6]
- Formatted ... [7]
- Formatted ... [3]
- Formatted ... [8]
- Formatted ... [10]
- Formatted ... [12]
- Formatted ... [9]
- Formatted ... [11]
- Formatted ... [13]
- Formatted ... [15]
- Formatted ... [17]
- Formatted ... [14]
- Formatted ... [16]
- Formatted ... [18]
- Formatted ... [20]
- Formatted ... [22]
- Formatted ... [19]
- Formatted ... [21]
- Formatted ... [23]
- Formatted ... [25]
- Formatted ... [27]
- Formatted ... [24]
- Formatted ... [26]
- Formatted ... [28]
- Formatted ... [30]
- Formatted ... [32]
- Formatted ... [29]
- Formatted ... [31]
- Formatted ... [33]
- Formatted ... [35]
- Formatted ... [37]
- Formatted ... [34]
- Formatted ... [36]
- Formatted ... [38]
- Formatted ... [40]
- Formatted ... [42]
- Formatted ... [39]
- Formatted ... [41]
- Formatted ... [43]
- Formatted ... [44]
- Formatted ... [46]
- Formatted ... [48]
- Formatted ... [45]
- Formatted ... [47]
- Formatted ... [49]
- Formatted ... [51]
- Formatted ... [53]
- Formatted ... [50]
- Formatted ... [52]
- Formatted ... [54]
- Formatted ... [56]
- Formatted ... [58]

19	$O + HO_2 \rightarrow OH + O_2$	5.9×10^{-11}	2	Sander et al. (2011)
20	$O + H_2O_2 \rightarrow OH + HO_2$	1.8×10^{-15}	2	Sander et al. (2011)
21	$H + O_2 + M \rightarrow HO_2 + M$	9.7×10^{-13}	*2	Sander et al. (2011)
22	$H + O_3 \rightarrow OH + O_2$	2.9×10^{-11}	2	Sander et al. (2011)
23	$H + HO_2 \rightarrow OH + OH$	7.2×10^{-11}	2	Sander et al. (2011)
24	$H + HO_2 \rightarrow O + H_2O$	1.6×10^{-12}	2	Sander et al. (2011)
25	$H + HO_2 \rightarrow H_2 + O_2$	6.9×10^{-12}	2	Sander et al. (2011)
26	$OH + O_3 \rightarrow HO_2 + O_2$	7.3×10^{-14}	2	Sander et al. (2011)
27	$OH + H_2 \rightarrow H_2O + H$	6.7×10^{-15}	2	Sander et al. (2011)
28	$OH + OH \rightarrow H_2O + O$	1.8×10^{-12}	2	Sander et al. (2011)
29	$OH + OH + M \rightarrow H_2O_2 + M$	6.4×10^{-12}	*2	Sander et al. (2011)
30	$OH + HO_2 \rightarrow H_2O + O_2$	1.1×10^{-10}	2	Sander et al. (2011)
31	$OH + H_2O_2 \rightarrow H_2O + HO_2$	1.8×10^{-12}	2	Sander et al. (2011)
32	$HO_2 + O_3 \rightarrow OH + O_2 + O_2$	1.9×10^{-15}	2	Sander et al. (2011)
33	$HO_2 + HO_2 (+M) \rightarrow H_2O_2 +$ $O_2 (+M)$	2.6×10^{-12}	2 + *2	Sander et al. (2011)
SO_x Chemistry				
34	$O + SO_2 + M \rightarrow SO_3 + M$	1.3×10^{-11}	*2	Sander et al. (2011)
35	$O_3 + SO_2 \rightarrow SO_3 + O_2$	2.0×10^{-22}	2	Sander et al. (2011)
36	$OH + S \rightarrow H + SO$	6.6×10^{-11}	2	Sander et al. (2011)
37	$OH + SO \rightarrow H + SO_2$	8.3×10^{-11}	2	Sander et al. (2011)
38	$OH + SO_2 + M \rightarrow HOSO_2 +$ M	9.6×10^{-13}	*2	Sander et al. (2011)
39	$HO_2 + SO_2 \rightarrow OH + SO_3$	1.0×10^{-18}	2	Sander et al. (2011)
40	$S + O_2 \rightarrow SO + O$	2.3×10^{-12}	2	Sander et al. (2011)
41	$S + O_3 \rightarrow SO + O_2$	1.2×10^{-11}	2	Sander et al. (2011)
42	$SO + O_2 \rightarrow SO_2 + O$	8.0×10^{-17}	2	Sander et al. (2011)
43	$SO + O_2 + M \rightarrow SO_3 + M$	Varies	*2	Sander et al. (2011)

Formatted	... [103]
Formatted	... [105]
Formatted	... [102]
Formatted	... [104]
Formatted	... [106]
Formatted	... [108]
Formatted	... [110]
Formatted	... [107]
Formatted	... [109]
Formatted	... [111]
Formatted	... [113]
Formatted	... [115]
Formatted	... [112]
Formatted	... [114]
Formatted	... [116]
Formatted	... [118]
Formatted	... [120]
Formatted	... [117]
Formatted	... [119]
Formatted	... [121]
Formatted	... [123]
Formatted	... [125]
Formatted	... [122]
Formatted	... [124]
Formatted	... [126]
Formatted	... [128]
Formatted	... [130]
Formatted	... [127]
Formatted	... [129]
Formatted	... [131]
Formatted	... [133]
Formatted	... [135]
Formatted	... [132]
Formatted	... [134]
Formatted	... [136]
Formatted	... [138]
Formatted	... [140]
Formatted	... [137]
Formatted	... [139]
Formatted	... [141]
Formatted	... [143]
Formatted	... [145]
Formatted	... [142]
Formatted	... [144]
Formatted	... [146]
Formatted	... [148]
Formatted	... [150]
Formatted	... [147]
Formatted	... [149]
Formatted	... [151]
Formatted	... [153]
Formatted	... [155]
Formatted	... [152]
Formatted	... [154]
Formatted	... [156]
Formatted	... [158]

44	$SO + O_3 \rightarrow SO_2 + O_2$	8.4×10^{-14}	2	Sander et al. (2011)
45	$HOSO_2 + O_2 \rightarrow HO_2 + SO_3$	4.3×10^{-13}	2	Sander et al. (2011)
46	$SO + HO_2 \rightarrow SO_2 + OH$	2.8×10^{-11}	2	DeMore et al. (1997)
47	$SO + SO_2 \rightarrow SO_2 + S$	8.3×10^{-16}	2	Chung et al. (1975)
48	$SO + O + M \rightarrow SO_2 + M$	1.3×10^{-11}	*2	Cobos et al. (1985)
49	$SO + SO_2 \rightarrow SO_2 + SO_2$	2.0×10^{-15}	2	Chung et al. (1975)
50	$S + S + M \rightarrow S_2 + M$	7.5×10^{-14}	*2	Pavlov and Kasting (2002)
51	$SO_2 + 2 H_2O \rightarrow aerosol$	2.9×10^{-31}	3 (special)	Sander et al. (2011)

Other

k_{out} Exit rate from cell 2.1×10^{-2} 1

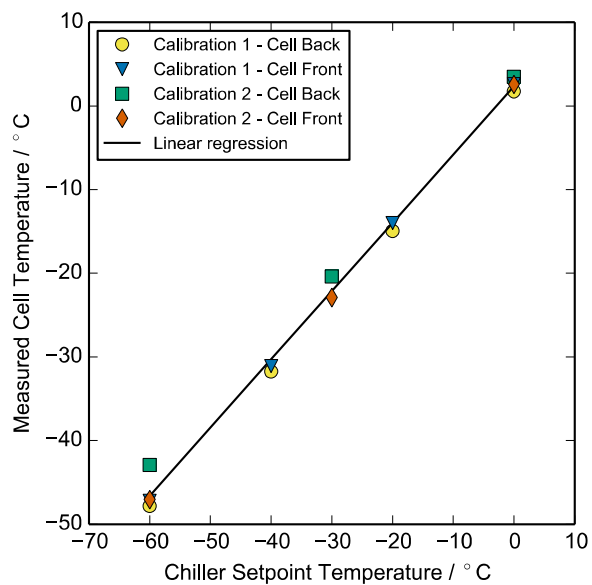
* Effective second order reactions based on falloff curves for $[M] = 2.5 \times 10^{19}$ and $M = N_2, O_2$. See sources for additional information.

Reaction Number	Reaction	Rate constant	Reaction Order	Source
Photochemical Reactions				
R4	$SO_2 + h\nu \rightarrow SO + O$	5.2×10^{-3}	1	Manatt and Lane (1993)
R9	$O_2 + h\nu \rightarrow O + O$	1.7×10^{-6}	1	Yoshino et al. (1988, 1992)
R10	$O_2 + h\nu \rightarrow O + O_2$	1.1×10^{-1}	1	Molina and Molina (1986)
O_x Chemistry				
R11	$O + O + M \rightarrow O_2 + M$	1.0×10^{-33}	3	Sander et al. (2011)
R12	$O + O_2 + M \rightarrow O_3 + M$	6.0×10^{-34}	3	Sander et al. (2011)
R13	$O + O_3 \rightarrow O_2 + O_2$	8.0×10^{-15}	2	Sander et al. (2011)
SO_x Chemistry				
R5	$SO + O_2 \rightarrow SO_2 + O$	8.0×10^{-11}	2	Sander et al. (2011)
R6	$SO + O_2 + M \rightarrow SO_3 + M$	Varies	3	
R7	$SO_2 + O + M \rightarrow SO_3 + M$	1.3×10^{-14}	*2	Sander et al. (2011)

- Formatted ... [229]
- Formatted ... [231]
- Formatted ... [228]
- Formatted ... [230]
- Formatted ... [232]
- Formatted ... [234]
- Formatted ... [236]
- Formatted ... [233]
- Formatted ... [235]
- Formatted ... [237]
- Formatted ... [239]
- Formatted ... [241]
- Formatted ... [238]
- Formatted ... [240]
- Formatted ... [242]
- Formatted ... [244]
- Formatted ... [246]
- Formatted ... [243]
- Formatted ... [245]
- Formatted ... [247]
- Formatted ... [249]
- Formatted ... [251]
- Formatted ... [248]
- Formatted ... [250]
- Formatted ... [252]
- Formatted ... [254]
- Formatted ... [256]
- Formatted ... [253]
- Formatted ... [255]
- Formatted ... [257]
- Formatted ... [259]
- Formatted ... [261]
- Formatted ... [258]
- Formatted ... [260]
- Formatted ... [262]
- Formatted ... [264]
- Formatted ... [266]
- Formatted ... [263]
- Formatted ... [265]
- Formatted ... [267]
- Formatted ... [268]
- Formatted ... [269]
- Formatted ... [270]
- Formatted ... [271]
- Formatted ... [272]
- Formatted ... [273]

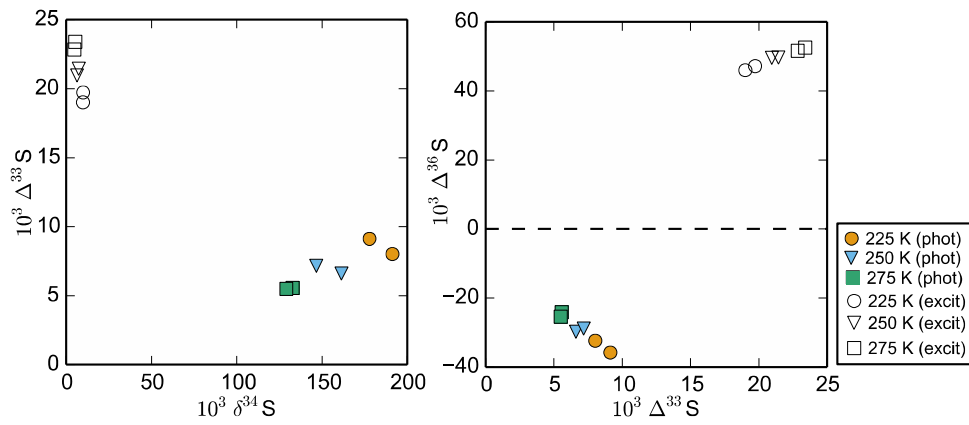
R8	$\text{SO} + \text{SO} \rightarrow \text{SO}_2 + \text{S}$	8.3×10^{-16}	2	Chung et al. (1975)
R14	$\text{SO} + \text{O} + \text{M} \rightarrow \text{SO}_2 + \text{M}$	1.3×10^{-11}	*2	Cobos et al. (1985)
R15	$\text{SO} + \text{O}_3 \rightarrow \text{SO}_2 + \text{O}_2$	8.4×10^{-14}	2	Sander et al. (2011)
R16	$\text{S} + \text{O}_2 \rightarrow \text{SO} + \text{O}$	2.3×10^{-12}	2	Sander et al. (2011)
R17	$\text{S} + \text{O}_3 \rightarrow \text{SO} + \text{O}_2$	1.2×10^{-14}	2	Sander et al. (2011)
Other				
k _{out}	Exit rate from cell	2.1×10^{-2}	1	

- 1 * Effective second-order reactions based on falloff curves for $[\text{M}] = 2.5 \times 10^{19}$ and $\text{M} = \text{N}_2, \text{O}_2$. See
- 2 sources for additional information.

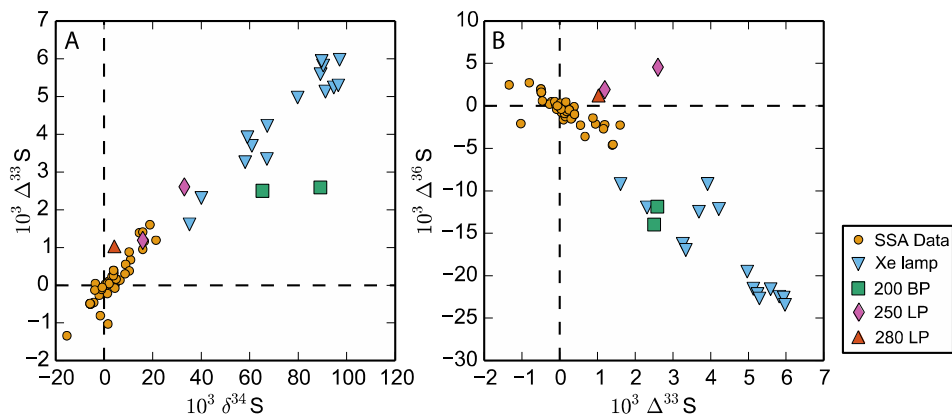


1
 2 Figure 1. Results of the temperature calibration for the temperature controlled photochemical
 3 reactor described in Section 2.1 The linear regression shown was used to calibrate the
 4 temperature within the cell based on the setpoint temperature of the chiller. The regression
 5 line is $(T_{Cell} / ^\circ\text{C}) = 0.8160 \times (T_{Chiller} / ^\circ\text{C}) + 2.3514$.

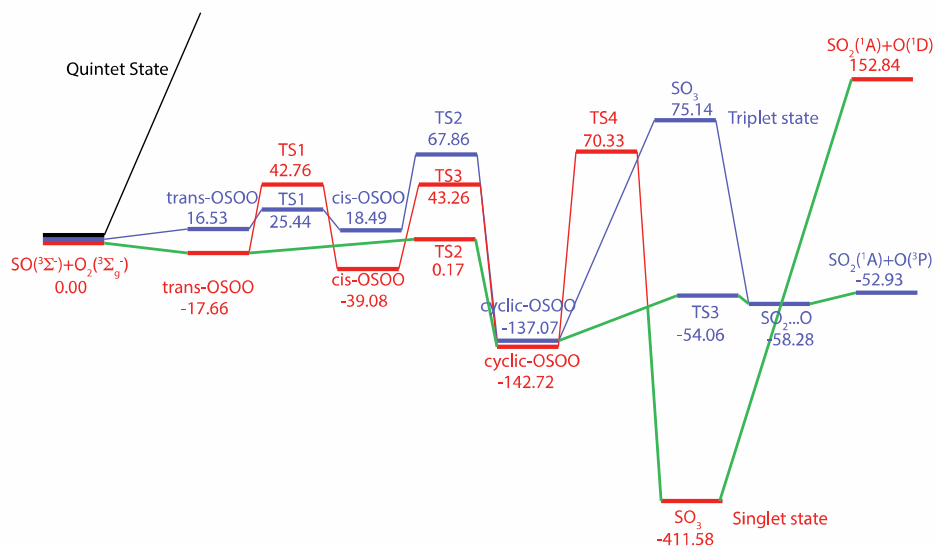
6



1
 2 Figure 2. Results of the temperature experiments for SO₂ photolysis and SO₂ photoexcitation
 3 (Section 2.2). Results from SO₂ photolysis experiments (phot) are shown in filled symbols
 4 and SO₂ photoexcitation experiments (excit) are in empty symbols.
 5

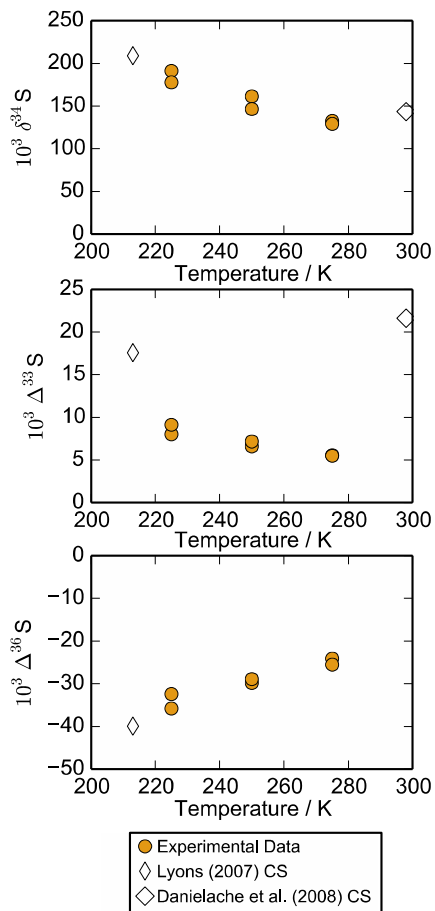


1
 2 Figure 3. Isotopic results of the $\text{SO}_2 + \text{O}_2$ experiments described in Section 2.3, compared with
 3 stratospheric sulfate aerosol samples (SSA Data) from Savarino et al. (2003), Baroni et al.
 4 (2007, 2008), Lanciki (2010), and Lanciki et al. (2012).
 5

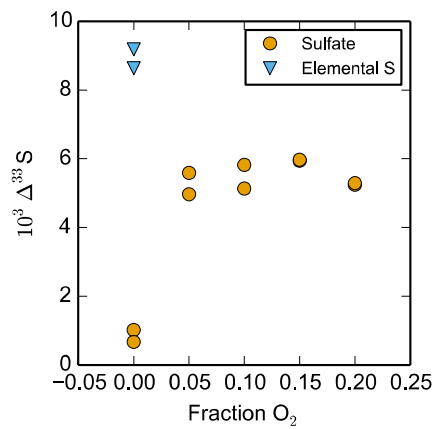


1
 2 Figure 4. Potential energy profiles on the singlet (red) and triplet (blue) potential energy
 3 surfaces for the SO₃ system obtained using B3LYP optimization followed by UCCSD(T)-
 4 F12a single point calculation, with the AVTZ basis set. The possible intersystem crossing
 5 pathway is depicted by the solid green line. All energies are given in kJ mole⁻¹ relative to the
 6 SO(³Σ⁻)+O₂(³Σ_g⁻) asymptote. The quintet (black) state is shown qualitatively due to its high
 7 energy.

8
 9

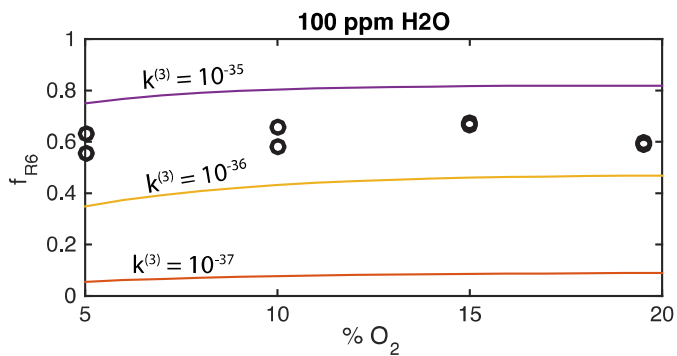
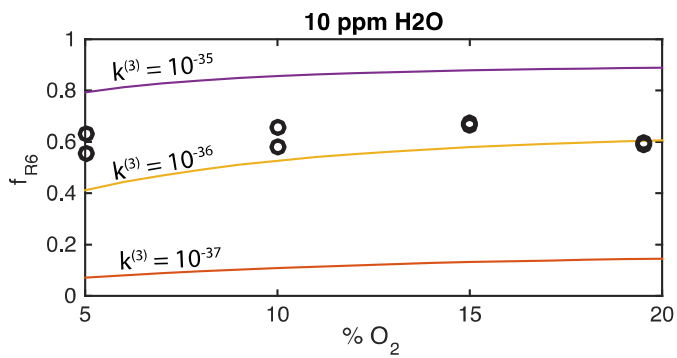
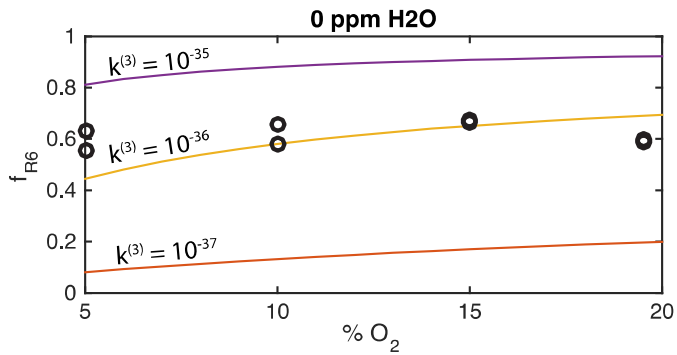


1
 2 Figure 5. Comparison of SO₂ photolysis temperature experiment results with predictions from
 3 isotopologue-specific absorption cross-sections (CS).
 4

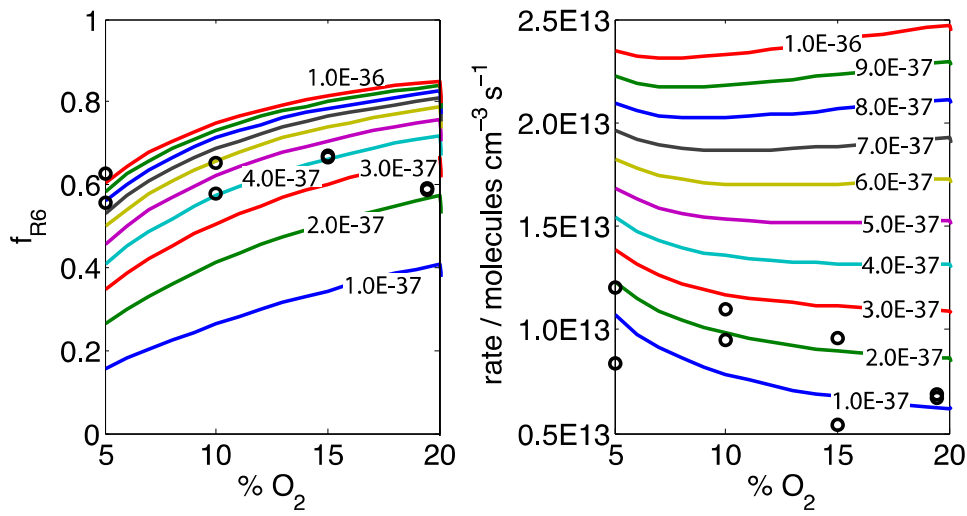


1
2 Figure 6. $\Delta^{33}\text{S}$ values of sulfate from the photolysis of SO_2 in the presence of O_2 compared
3 with elemental sulfur and sulfate from SO_2 photolysis in the absence of O_2 . Conditions are
4 described in Section 4.3 and Table 4.
5

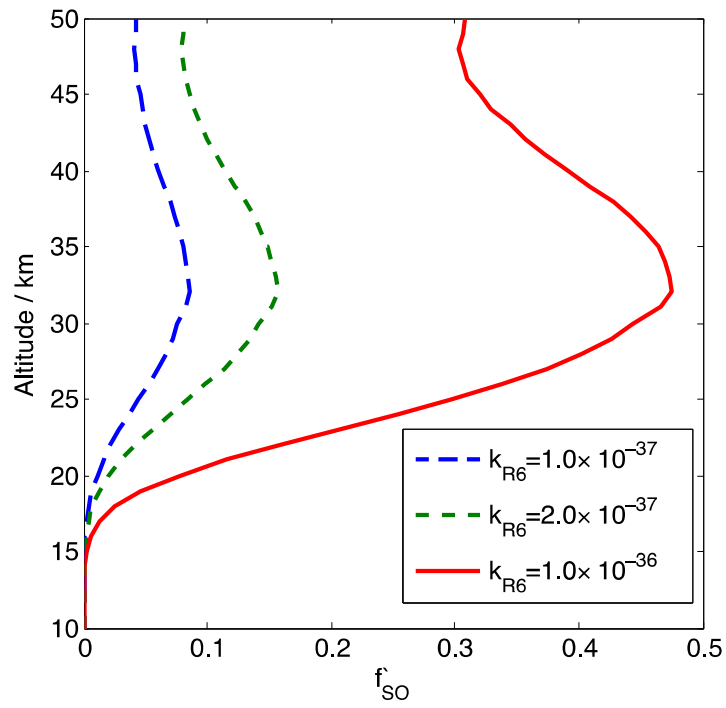
Formatted: Font: (Default) Times New Roman, Not Bold



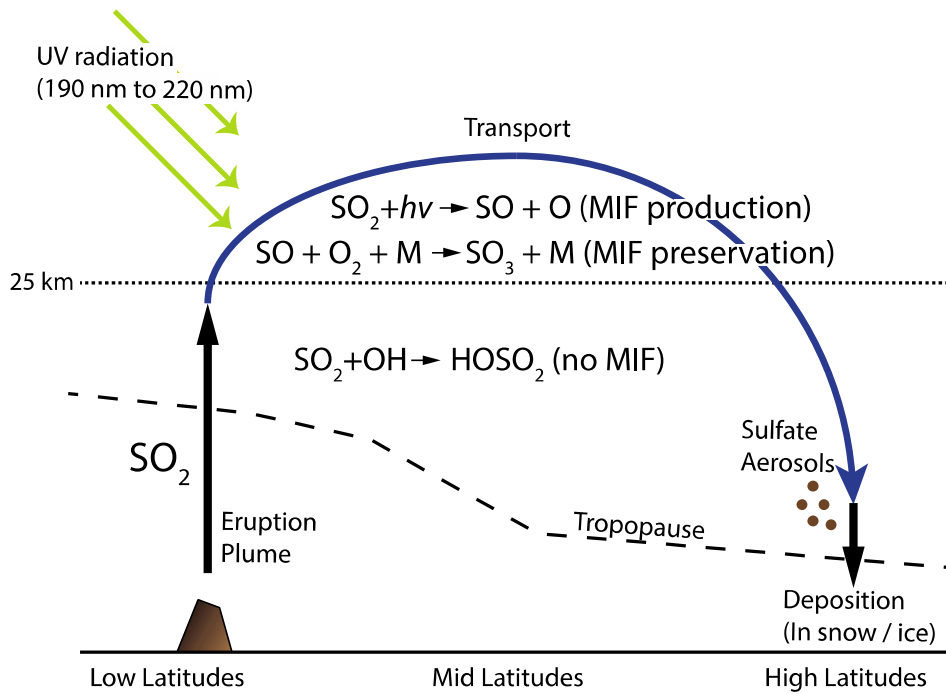
1



1
 2 Figure 7. Results of kinetic model (Section 4.4, Table 9) compared to experimental data
 3 (circles) for f_{R6} (Equation 5) versus fraction of SO₃ formed from R6 in the model ~~(left), as~~
 4 ~~well as total SO₃ formation rate (right).~~ Contours on the plot are labeled with the value of rate
 5 constant k_{R6} input into the model for a given run. Experimental data is plotted as black
 6 circles. The model was run for three input values of H₂O concentration: 0 ppmv (top), 10
 7 ppmv (middle), and 100 ppmv (bottom).



1
 2 Figure 8. Fraction of sulfate derived from reaction channel R6 (f_{SO}) as a function of altitude for
 3 different values of k_{R6} .
 4



1
 2 Figure 9. Schematic illustration of the production and preservation of mass-independent
 3 fractionation (MIF) in sulfur isotopes following explosive volcanic eruptions. Low latitude
 4 eruptions such as Pinatubo (1991) inject large amounts of SO_2 into the stratosphere. Through
 5 stratospheric transport, it is brought to altitudes where SO_2 photolysis can occur, producing
 6 large MIF signatures. The product of SO_2 photolysis, SO , is preserved via termolecular
 7 reaction with O_2 . The resulting SO_3 forms sulfate aerosols, which are deposited at high
 8 latitudes in polar snow and ice core records. SO_2 oxidation below around 25 km is
 9 dominantly by OH , which is a mass-dependent process.

10

12/12/2014 3:34:00 PM

12/12/2014 3:34:00 PM

12/12/2014 3:34:00 PM

12/12/2014 3:34:00 PM

12/12/2014 3:34:00 PM

12/12/2014 3:34:00 PM

12/12/2014 3:34:00 PM

12/12/2014 3:34:00 PM

12/12/2014 3:34:00 PM

12/12/2014 3:34:00 PM

12/12/2014 3:34:00 PM

12/12/2014 3:34:00 PM

12/12/2014 3:34:00 PM

12/12/2014 3:34:00 PM

12/12/2014 3:34:00 PM

12/12/2014 3:34:00 PM

12/12/2014 3:34:00 PM

12/12/2014 3:34:00 PM

12/12/2014 3:34:00 PM

12/12/2014 3:34:00 PM

12/12/2014 3:34:00 PM

12/12/2014 3:34:00 PM

12/12/2014 3:34:00 PM

12/12/2014 3:34:00 PM

12/12/2014 3:34:00 PM

12/12/2014 3:34:00 PM

12/12/2014 3:34:00 PM

12/12/2014 3:34:00 PM

12/12/2014 3:34:00 PM

12/12/2014 3:34:00 PM

12/12/2014 3:34:00 PM

12/12/2014 3:34:00 PM

12/12/2014 3:34:00 PM

12/12/2014 3:34:00 PM

12/12/2014 3:34:00 PM

12/12/2014 3:34:00 PM

12/12/2014 3:34:00 PM

12/12/2014 3:34:00 PM

12/12/2014 3:34:00 PM

12/12/2014 3:34:00 PM

12/12/2014 3:34:00 PM

12/12/2014 3:34:00 PM

12/12/2014 3:34:00 PM

12/12/2014 3:34:00 PM

12/12/2014 3:34:00 PM

12/12/2014 3:34:00 PM

12/12/2014 3:34:00 PM

12/12/2014 3:34:00 PM

12/12/2014 3:34:00 PM

12/12/2014 3:34:00 PM

12/12/2014 3:34:00 PM

12/12/2014 3:34:00 PM

12/12/2014 3:34:00 PM

12/12/2014 3:34:00 PM

12/12/2014 3:34:00 PM

12/12/2014 3:34:00 PM

12/12/2014 3:34:00 PM

12/12/2014 3:34:00 PM

12/12/2014 3:34:00 PM

12/12/2014 3:34:00 PM

12/12/2014 3:34:00 PM

12/12/2014 3:34:00 PM

12/12/2014 3:34:00 PM

12/12/2014 3:34:00 PM

12/12/2014 3:34:00 PM

12/12/2014 3:34:00 PM

12/12/2014 3:34:00 PM

12/12/2014 3:34:00 PM

12/12/2014 3:34:00 PM

12/12/2014 3:34:00 PM

12/12/2014 3:34:00 PM

12/12/2014 3:34:00 PM

12/12/2014 3:34:00 PM

12/12/2014 3:34:00 PM

12/12/2014 3:34:00 PM

12/12/2014 3:34:00 PM

12/12/2014 3:34:00 PM

12/12/2014 3:34:00 PM

12/12/2014 3:34:00 PM

12/12/2014 3:34:00 PM

12/12/2014 3:34:00 PM

12/12/2014 3:34:00 PM

12/12/2014 3:34:00 PM

12/12/2014 3:34:00 PM

12/12/2014 3:34:00 PM

12/12/2014 3:34:00 PM

12/12/2014 3:34:00 PM

12/12/2014 3:34:00 PM

12/12/2014 3:34:00 PM

12/12/2014 3:34:00 PM

12/12/2014 3:34:00 PM

12/12/2014 3:34:00 PM

12/12/2014 3:34:00 PM

12/12/2014 3:34:00 PM

12/12/2014 3:34:00 PM

12/12/2014 3:34:00 PM

12/12/2014 3:34:00 PM

12/12/2014 3:34:00 PM

12/12/2014 3:34:00 PM

12/12/2014 3:34:00 PM

12/12/2014 3:34:00 PM

12/12/2014 3:34:00 PM

12/12/2014 3:34:00 PM

12/12/2014 3:34:00 PM

12/12/2014 3:34:00 PM

12/12/2014 3:34:00 PM

12/12/2014 3:34:00 PM

12/12/2014 3:34:00 PM

12/12/2014 3:34:00 PM

12/12/2014 3:34:00 PM

12/12/2014 3:34:00 PM

12/12/2014 3:34:00 PM

12/12/2014 3:34:00 PM

12/12/2014 3:34:00 PM

12/12/2014 3:34:00 PM

12/12/2014 3:34:00 PM

12/12/2014 3:34:00 PM

12/12/2014 3:34:00 PM

12/12/2014 3:34:00 PM

12/12/2014 3:34:00 PM

12/12/2014 3:34:00 PM

12/12/2014 3:34:00 PM

12/12/2014 3:34:00 PM

12/12/2014 3:34:00 PM

12/12/2014 3:34:00 PM

12/12/2014 3:34:00 PM

12/12/2014 3:34:00 PM

12/12/2014 3:34:00 PM

12/12/2014 3:34:00 PM

12/12/2014 3:34:00 PM

12/12/2014 3:34:00 PM

12/12/2014 3:34:00 PM

12/12/2014 3:34:00 PM

12/12/2014 3:34:00 PM

12/12/2014 3:34:00 PM

12/12/2014 3:34:00 PM

12/12/2014 3:34:00 PM

12/12/2014 3:34:00 PM

12/12/2014 3:34:00 PM

12/12/2014 3:34:00 PM

12/12/2014 3:34:00 PM

12/12/2014 3:34:00 PM

12/12/2014 3:34:00 PM

12/12/2014 3:34:00 PM

12/12/2014 3:34:00 PM

12/12/2014 3:34:00 PM

12/12/2014 3:34:00 PM

12/12/2014 3:34:00 PM

12/12/2014 3:34:00 PM

12/12/2014 3:34:00 PM

12/12/2014 3:34:00 PM

12/12/2014 3:34:00 PM

12/12/2014 3:34:00 PM

12/12/2014 3:34:00 PM

12/12/2014 3:34:00 PM

12/12/2014 3:34:00 PM

12/12/2014 3:34:00 PM

12/12/2014 3:34:00 PM

12/12/2014 3:34:00 PM

12/12/2014 3:34:00 PM

12/12/2014 3:34:00 PM

12/12/2014 3:34:00 PM

12/12/2014 3:34:00 PM

12/12/2014 3:34:00 PM

12/12/2014 3:34:00 PM

12/12/2014 3:34:00 PM

12/12/2014 3:34:00 PM

12/12/2014 3:34:00 PM

12/12/2014 3:34:00 PM

12/12/2014 3:34:00 PM

12/12/2014 3:34:00 PM

12/12/2014 3:34:00 PM

12/12/2014 3:34:00 PM

12/12/2014 3:34:00 PM

12/12/2014 3:34:00 PM

12/12/2014 3:34:00 PM

12/12/2014 3:34:00 PM

12/12/2014 3:34:00 PM

12/12/2014 3:34:00 PM

12/12/2014 3:34:00 PM

12/12/2014 3:34:00 PM

12/12/2014 3:34:00 PM

12/12/2014 3:34:00 PM

12/12/2014 3:34:00 PM

12/12/2014 3:34:00 PM

12/12/2014 3:34:00 PM

12/12/2014 3:34:00 PM

12/12/2014 3:34:00 PM

12/12/2014 3:34:00 PM

12/12/2014 3:34:00 PM

12/12/2014 3:34:00 PM

12/12/2014 3:34:00 PM

12/12/2014 3:34:00 PM

12/12/2014 3:34:00 PM

12/12/2014 3:34:00 PM

12/12/2014 3:34:00 PM

12/12/2014 3:34:00 PM

12/12/2014 3:34:00 PM

12/12/2014 3:34:00 PM

12/12/2014 3:34:00 PM

12/12/2014 3:34:00 PM

12/12/2014 3:34:00 PM

12/12/2014 3:34:00 PM

12/12/2014 3:34:00 PM

12/12/2014 3:34:00 PM

12/12/2014 3:34:00 PM

12/12/2014 3:34:00 PM

12/12/2014 3:34:00 PM

12/12/2014 3:34:00 PM

12/12/2014 3:34:00 PM

12/12/2014 3:34:00 PM

12/12/2014 3:34:00 PM

12/12/2014 3:34:00 PM

12/12/2014 3:34:00 PM

12/12/2014 3:34:00 PM

12/12/2014 3:34:00 PM

12/12/2014 3:34:00 PM

12/12/2014 3:34:00 PM

12/12/2014 3:34:00 PM

12/12/2014 3:34:00 PM

12/12/2014 3:34:00 PM

12/12/2014 3:34:00 PM

12/12/2014 3:34:00 PM

12/12/2014 3:34:00 PM

12/12/2014 3:34:00 PM

12/12/2014 3:34:00 PM

12/12/2014 3:34:00 PM

12/12/2014 3:34:00 PM

12/12/2014 3:34:00 PM

12/12/2014 3:34:00 PM

12/12/2014 3:34:00 PM

12/12/2014 3:34:00 PM

12/12/2014 3:34:00 PM

12/12/2014 3:34:00 PM

12/12/2014 3:34:00 PM

12/12/2014 3:34:00 PM

12/12/2014 3:34:00 PM

12/12/2014 3:34:00 PM

12/12/2014 3:34:00 PM

12/12/2014 3:34:00 PM

12/12/2014 3:34:00 PM

12/12/2014 3:34:00 PM

12/12/2014 3:34:00 PM

12/12/2014 3:34:00 PM

12/12/2014 3:34:00 PM

12/12/2014 3:34:00 PM

12/12/2014 3:34:00 PM

12/12/2014 3:34:00 PM

12/12/2014 3:34:00 PM

12/12/2014 3:34:00 PM

12/12/2014 3:34:00 PM

12/12/2014 3:34:00 PM

12/12/2014 3:34:00 PM

12/12/2014 3:34:00 PM

12/12/2014 3:34:00 PM

12/12/2014 3:34:00 PM

12/12/2014 3:34:00 PM

12/12/2014 3:34:00 PM

12/12/2014 3:34:00 PM

12/12/2014 3:34:00 PM

12/12/2014 3:34:00 PM

12/12/2014 3:34:00 PM

12/12/2014 3:34:00 PM

12/12/2014 3:34:00 PM

12/12/2014 3:34:00 PM

12/12/2014 3:34:00 PM

12/12/2014 3:34:00 PM

12/12/2014 3:34:00 PM

12/12/2014 3:34:00 PM

12/12/2014 3:34:00 PM

12/12/2014 3:34:00 PM

12/12/2014 3:34:00 PM

12/12/2014 3:34:00 PM

12/12/2014 3:34:00 PM

12/12/2014 3:34:00 PM

12/12/2014 3:34:00 PM

12/12/2014 3:34:00 PM

12/12/2014 3:34:00 PM

12/12/2014 3:34:00 PM

12/12/2014 3:34:00 PM

12/12/2014 3:34:00 PM

12/12/2014 3:34:00 PM

12/12/2014 3:34:00 PM

12/12/2014 3:34:00 PM

12/12/2014 3:34:00 PM

12/12/2014 3:34:00 PM

12/12/2014 3:34:00 PM

12/12/2014 3:34:00 PM

12/12/2014 3:34:00 PM

12/12/2014 3:34:00 PM

12/12/2014 3:34:00 PM

12/12/2014 3:34:00 PM

12/12/2014 3:34:00 PM

12/12/2014 3:34:00 PM

12/12/2014 3:34:00 PM

12/12/2014 3:34:00 PM

12/12/2014 3:34:00 PM